EBioMedicine 63 (2021) 103191

Contents lists available at ScienceDirect

EBioMedicine

journal homepage: www.elsevier.com/locate/ebiom

Research paper

Dnmt3b catalytic activity is critical for its tumour suppressor function in lymphomagenesis and is associated with c-Met oncogenic signalling

Katarina Lopusna[a,#], Pawel Nowialis[a,#], Jana Opavska[a], Ajay Abraham[a], Alberto Riva[b], Rene Opavsky[a,*]

[a] Department of Anatomy and Cell Biology, University of Florida College of Medicine, 2033 Mowry Rd, CGRC 258, Gainesville, FL 32610, United States
[b] ICBR Bioinformatics, Cancer and Genetics Research Complex, University of Florida, P.O. Box 103622. Gainesville, FL 32610, United States

ARTICLE INFO

Article History:
Received 4 August 2020
Revised 10 December 2020
Accepted 14 December 2020
Available online xxx

Keywords:
Lymphomagenesis
DNA methyltransferase
Epigenetic
Tumour suppressor
Catalytic activity
Mouse model
DNA methylation

ABSTRACT

Background: DNA methylation regulates gene transcription in many physiological processes in mammals including development and haematopoiesis. It is catalysed by several DNA methyltransferases, including Dnmt3b that mediates both methylation-dependant and independent gene repression. Dnmt3b is critical for mouse embryogenesis and functions as a tumour suppressor in haematologic malignancies in mice. However, the extent to which Dnmt3b's catalytic activity (CA) is involved in development and cancer is unclear.
Methods: We used a mouse model expressing catalytically inactive Dnmt3b (Dnmt3b^{CI}) to study a role of Dnmt3b's CA in development and cancer. We utilized global approaches including Whole-genome Bisulfite sequencing and RNA-seq to analyse DNA methylation and gene expression to identify putative targets of Dnmt3b's CA. To analyse postnatal development and haematopoiesis, we used tissue staining, histological and FACS analysis. To determine potential involvement of selected genes in lymphomagenesis, we used overexpression and knock down approaches followed by *in vitro* growth assays.
Findings: We show that mice expressing Dnmt3b^{CI} only, survive postnatal development and develop ICF (the immunodeficiency-centromeric instability-facial anomalies) -like syndrome. The lack of Dnmt3b's CA promoted fibroblasts transformation *in vitro*, accelerated MLL-AF9 driven Acute Myeloid Leukaemia and MYC-induced T-cell lymphomagenesis *in vivo*. The elimination of Dnmt3b's CA resulted in decreased methylation of c-Met promoter and its upregulation, activated oncogenic Met signalling, Stat3 phosphorylation and upregulation of Lin28b promoting lymphomagenesis.
Interpretation: Our data demonstrates that Dnmt3b's CA is largely dispensable for mouse development but critical to prevent tumourigenesis by controlling events involved in cellular transformation.
Funding: This study was supported by Department of Anatomy and Cell Biology and Cancer Centre at the University of Florida start-up funds, NIH/NCI grant 1R01CA188561-01A1 (R.O.).

1. Introduction

DNA methylation is an epigenetic modification that regulates gene transcription in mammalian cells, particularly when present in gene promoters. It is often associated with H3K9me3 and H3K27me3 histone modifications and contributes to gene repression [1,2]. DNA methylation is involved in various physiological processes, including development, X chromosome inactivation, genomic imprinting, differentiation and hematopoiesis and its deregulation in humans contributes to the pathogenesis of immune disorders, haematologic malignancies and cancer [3,4].

Three main DNA methyltransferases (Dnmt1, Dnmt3a, Dnmt3b; Dnmts) and one cofactor (Dnmt3L) are involved in catalysing DNA methylation in mammals.

While all Dnmts participate in genome-wide methylation, they do have unique functions. Dnmt3a and Dnmt3b are mostly *de novo* enzymes characterized by ability to methylate naked DNA and high methylation activity during early embryogenesis [5]. In contrast, Dnmt1 has a high affinity for hemi-methylated sites and functions in the maintenance during cellular division to ensure accurate transfer of epigenetic methylation marks to progeny cells [6,7]. Dnmt3L lacks catalytic activity but functions as an accessory protein critical for induction of methylation by linking Dnmt3a/b to chromatin through unmethylated H3 lysine 4 [8].

* Corresponding author.
E-mail address: ropavsky@ufl.edu (R. Opavsky).
# These authors contributed equally to this work

https://doi.org/10.1016/j.ebiom.2020.103191

Research in Context

Evidence before this study

Dnmt3b is a tumour suppressor in various haematologic malignancies including MYC-induced T- and B-cell lymphomas and in Acute Myeloid Leukaemia that is also critical for normal mouse development. These data were obtained utilizing gene knockouts that eliminated Dnmt3b protein thus removing Dnmt3b's catalytic, accessory and repressive functions. We have previously shown that Dnmt3b's catalytic activity is dispensable for pre-natal development because remaining accessory and repressive functions were sufficient to rescue mouse embryogenesis but its role in post-natal development and tumourigenesis was unclear.

Added value of this study

We demonstrated that Dnmt3b's catalytic activity is largely dispensable for postnatal development with mice surviving, but developing ICF-like syndrome. Inactivation of Dnmt3b's catalytic activity promotes cellular transformation of fibroblasts and myeloid cells *in vitro* and *in vivo* and was associated with upregulation of c-Met-proto-oncogene signalling and acceleration of MYC-induced T-cell lymphomagenesis. Altogether, our data show that Dnmt3b is a multifunctional protein involved in control of genes important to prevent ICF and tumourigenesis.

Implications of all the available evidence

Our data provide a direct genetic evidence that Dnmt3b's catalytic activity is critical in pathogenesis of mouse haematologic malignancies thus providing mechanistic insight into biological basis of its tumour suppressor function. A consequence of this finding is that through methylation, Dnmt3b's catalytic activity is associated with genes causatively contributing to tumourigenesis, including c-Met. Our findings pave the way for a more systematic analysis of oncogenic MET signalling contribution to pathogenesis of human disease.

In addition to catalytic activity (CA), Dnmts can repress transcription independently of methylation *e.g.* through association with HDACs [9-11]. Dnmt3L and Dnmt3b also possess accessory function (AF) that consist of the ability to recruit other Dnmts to genomic loci to catalyse methylation [8,12,13].

Dnmt3b is involved in *de novo* methylation and repression of germ line genes and X chromosome inactivation and its knockout is embryonically lethal at E11.5−15.5 [5,14]. Human DNMT3B plays a role in a rare recessive autosomal disorder - the immunodeficiency-centromeric instability-facial anomalies (ICF) syndrome – characterized by mild facial anomalies, cognitive impairment, recurrent infections, a lack of memory B-cells in peripheral blood and variable cellular deficiencies [15,16].

About 60% of ICF patients has compound heterozygotes mutations in the DNMT3B usually targeting the catalytic domain [17,18].

DNMT3B is also mutated in a subset of haematologic malignancies including Cutaneous T-cell Lymphomas (CTCLs) and B-cell Lymphomas (BCLs) [19,20]. Studies in mice showed that Dnmt3b is a tumour suppressor (TS) in various haematologic malignancies including MYC-induced T- and B-cell lymphomas and in acute myeloid leukaemia induced by MLL-AF9 overexpression [21-25]. In these settings, gene knockouts eliminated Dnmt3b protein thus removing Dnmt3b's CA, AF and repressive functions. We have previously reported that Dnmt3b's CA is dispensable for pre-natal development because remaining accessory and repressive functions were sufficient to rescue mouse embryogenesis. The extent to which various Dnmt3b's activities play a role in post-natal development, ICF and tumourigenesis remains unclear.

Here we used mice expressing catalytically inactive Dnmt3b ($Dnmt3b^{CI}$) and found that CA is largely dispensable for postnatal development with mice surviving but developing ICF-like syndrome in mice. The inactivation of Dnmt3b's CA promoted cellular transformation *in vitro* and *in vivo* in fibroblasts and myeloid cells, is associated with upregulation of proto-oncogene c-Met signalling and accelerated MYC-induced T-cell lymphomagenesis (MTCL). Altogether, our data show that Dnmt3b is a multifunctional protein involved in control of genes important to prevent ICF and tumourigenesis.

2. Methods

2.1. Mouse studies

Mice harbouring conventional knock-in mutations (P656V and C657D) in Dnmt3b coding sequence (Dnmt3bCI) were generated as described before [13]. PCR-based genotyping was carried out as previously [13]. *EμSRα-tTA;Teto-MYC* mice were obtained from D.W. Felsher (Stanford University). All experiments were performed using mice of FVB/NJ background. Mice of appropriate genotypes were monitored and harvested at the terminal stage, as determined by overall health. Genomic DNA isolated from mouse tails was used in PCR-based genotyping. For developmental studies, organ weight and cellularity of thymus, spleen, and lymph nodes were compared between $Dnmt3b^{+/+}$ and $Dnmt3b^{CI/CI}$ littermates. For long term observational studies $Dnmt3b^{+/+}$ and $Dnmt3b^{CI/CI}$ littermates were observed for more than 14 months. For MYC-induced T-cell lymphomagenesis studies, a survival in cohorts of *EμSRα-tTA;Teto-MYC;*$Dnmt3b^{+/+}$ (termed *MYC;*$Dnmt3b^{+/+}$), *EμSRα-tTA;Teto-MYC;*$Dnmt3b^{+/CI}$ (termed *MYC;*$Dnmt3b^{+/CI}$) and *EμSRα-tTA;Teto-MYC;*$Dnmt3b^{CI/CI}$ (termed *MYC;*$Dnmt3b^{CI/CI}$) mice was monitored. Mice were harvested at the terminal stage, as determined by overall health. All mice were housed in a pathogen-free barrier facility at the UF.

2.2. Ethics

All experimental animal procedures were approved by the Institutional Animal Care and Use Committee (IACUC) at the University of Florida under protocol number 201909589 and complied with all relevant ethical regulations for animal testing and research.

2.3. Adoptive transfer

Adoptive transfer experiment was performed with foetal liver cells isolated from 15.5-days-old embryos of *EμSRα-tTA;Teto-MYC;*$Dnmt3b^{+/+}$ and *EμSRα-tTA;Teto-MYC;*$Dnmt3b^{CI/CI}$ mice. Eight-week old FVB mice were used as recipients and were irradiated twice with 550 rads at 4 h intervals with Gammacell 40 ^{137}Cs irradiator. Mice were injected via the tail vein with 1×10^6 cells and observed for a period of 160 days. Development of T-cell lymphomas was confirmed by FACS analysis.

2.4. Plasmid DNA, cell cultures and lentiviruses

Lentiviral vectors pLV-EF1A-eGFP and pLV-mDnmt3b-FLAG-EF1A-mCherry were obtained from VectorBuilder. Lentiviral vector pLenti-cyto-Met-GFP (#37561) and retroviral vectors MSCV-H-Ras-VI2-IRES-GFP (#18780) and MSCV-cMyc-IRES-RFP (#35395) were obtained from Addgene. Retroviral vector MSCV-(myc)-Lin28b-(flag)-IRES-eGFP was generated as described previously [11]. Lentiviral small hairpin RNA (shRNA) constructs TRCN0000040043−5 (c-MET) and TRCN0000143619, TRCN0000122599 and TRCN0000122191 (LIN28B) from the Thermo

Scientific TRC shRNA library TRC—Hs1.0 (Human) were obtained from the UF's Lenti-shRNA Core Facility.

Lenti-XTM 293T Cell Line was purchased from Takara (#632180, Clontech). Human HUT-78 (# TIB-161, RRID:CVCL_0337) and HH (# CRL-2105, RRID:CVCL_1280) cells were obtained from the American Type Culture Collection (ATCC). Cell line was periodically checked for karyotype and tested for mycoplasma contamination. Only early passages were used. Mouse MYC-induced T-cell lymphoma line was established as described before [13,21]. Cells were maintained in DMEM or RPMI 1640 (Invitrogen) containing 10% foetal bovine serum. Cell lines were cultured at 37 °C in a humidified 5% CO2 atmosphere and were passaged according to recommendations.

To generate lentiviruses, 293T cells were seeded in 100 mm tissue culture plate to obtain ~80–90% confluence and transfected with plasmid DNA and packaging plasmids psPAX2 and pMD2.G at ratio 1:0.65:0.35 using 70 μg of polyethylenimine (PEI) (Polysciences). To generate retroviruses, Phoenix Eco cells were seeded in 100 mm tissue culture plate to obtain ~80–90% confluence and transfected with 12 μg of plasmid DNA. Virus was collected 48–96 h post transfection. Transduction was performed as described previously [21] using Polybrene Infection / Transfection Reagent (Sigma). Efficiency of transduction was determined by measuring percentage of EGFP+, RFP+ or mCherry+ cells by FACS.

For shRNA experiments, transduced HH and HUT-78 cell lines were first selected with puromycin (2.5 μg/ml) for 48 h. The growth of cells was then analysed using MTT assay (Thermo Fisher Scientific, USA) according to manufacturer's instructions. Briefly, cells were seeded at 40 $\times$ 10^3, 25 $\times$ 10^3 and 10 $\times$ 10^3 cells/well into 96 well microtiter plates in RPMI with 10% foetal bovine serum and grown for 2–6 days. Thereafter, the cells were treated with 3-[4,5-*dimethylthiazol*-2-*yl*]–2,5-diphenyltratrazolium bromide. Four hours later, all of the medium was aspirated from the wells. The remaining formazan crystals were dissolved in DMSO and the absorbence was measured at 570 nm using a 96 well microplate reader CLARIOstar® high-performance monochromator multimode microplate reader (BMG LABTECH, Ortenberg, Germany). Cells transduced with *scrambled* negative control shRNA served as a negative control.

2.5. MEFs transformation and colony formation assay

MEFs were isolated from E13.5 *Dnmt3b*$^{+/+}$ and *Dnmt3b*$^{Cl/Cl}$ embryos generated from interbreeding of *Dnmt3b*$^{+/Cl}$ mice using standard methods. All cells were cultured in DMEM with 10% foetal bovine serum. MEFs were transduced with viruses carrying vector encoding Myc and H-Ras^{V12} or control vector. Transduction efficiency was determined by percentage of RFP+ EGFP+ double positive cells as measured by FACS and was typically $\geq$ 95%. Dnmt3b expression in *Dnmt3b*$^{Cl/Cl}$ MEFs was achieved by transducing cells with lentiviruses encoding *wild-type* Dnmt3b or control vector followed by transduction with lentiviruses encoding Myc and H-Ras^{V12}. For colony formation assay, the transformed *Dnmt3b*$^{+/+}$ and *Dnmt3b*$^{Cl/Cl}$ MEFs were seeded at 3 different dilutions (25 $\times$ 10^3, 10 $\times$ 10^3 and 3 $\times$ 10^3 cells/10 cm^2 plate. The cells were stained with 0.5% crystal violet 7–10 days after plating. Colonies were counted directly on the plate. For *in vivo* study, transformed *Dnmt3b*$^{+/+}$ and *Dnmt3b*$^{Cl/Cl}$ MEFs (2.5 $\times$ 10^6 cells/ site) were injected subcutaneously into the right and left shoulders and hips of each 8–10-wk-old athymic nude mouse. Tumours that developed in these mice were harvested 10 days after injection.

2.6. Skeletal staining

For cranium staining mice heads were skinned and macerated in 2% KOH for 3 days. Eviscerated skulls were stained with 0.005% Alizarin Red (Sigma-Aldrich, A5533) solution for 4 days and washed with 1% KOH for one day to remove excess staining. Skeletons were transferred to glycerol and photographed using Zeiss Stemi 305 CAM Digital Stereo Zoom Microscope (Carl Zeiss, Inc., Thornwood, NY).

2.7. Immunoblotting

Western blots were performed as previously described [21], using the following antibodies detecting: Akt (cat.# 4691, Cell signalling, dilution 1:1000), Dnmt1 (cat.# ab188453, Abcam; dilution 1:500), Dnmt3a (cat.# SC-20703, Santa Cruz; dilution 1:1000), Dnmt3b (cat.# PA1–884, Thermo Fisher; dilution 1:1000), Stat3 (cat.# SC-8019, Santa Cruz; dilution 1:500), P-Stat3 (cat.# 9145, Cell signalling, dilution 1:1000), Stat5 (cat.# 25656, Cell signalling, dilution 1:1000), P-Stat5 (cat.# 9359, Cell signalling, dilution 1:1000), mouse c-Met (cat.# SC-8057; Santa Cruz; dilution 1:500), c-Myc (cat.# SC-40, Santa Cruz; dilution 1:1000), Hsc-70 (cat.# SC-7298, Santa Cruz; dilution 1:10000), Lin28b (cat.# SC-293120, Santa Cruz; dilution 1:500), h-Ras (cat.# SC-520, Santa Cruz, dilution 1:1000) and β-actin (cat.# SC-130657, Santa Cruz; dilution 1:1000).

2.8. Flow cytometry (FACS)

Freshly isolated single-cell suspensions were prepared from thymi, spleens, bone marrow, tumour masses or cell cultures. Red blood cells were lysed using Ammonium–chloride–potassium lysis buffer. Cells were stained with BioLegend antibodies for 30 min in 100 μl volume. For experiments with mouse bone marrow, lineage cocktails included antibodies against CD4, CD8, TCR-β, CD11b, CD19, B220, CD3, CD5, NK1.1, GR-1 and TER119 to define lineage positive populations. LSK cells (Lineage negative, Sca-1+,c-kit+), myeloid progenitors (Lineage negative, Sca-1-,c-kit+), Pre/Pro-B-cells (B220+IgM-IgD-) in bone marrow, immature B-cells (B220+IgM+IgD-), recirculating B-cells in BM (B220+IgM+IgD+), transitional T1 B-cells (CD19+B220+IgM+IgD-) in spleen, mature B-cells (CD19+B220+IgD+IgM+) in spleen, total B-cells in spleen (CD19+B220+), myeloid cells in spleen (CD11b+CD5-), double negative T-cells (CD4-CD8-) – DN1 (CD44+CD25-), DN2 (CD44+CD25+), DN3 (CD44-CD25+), DN4 (CD44-CD25-) in thymus, double positive T-cells (CD4+CD8+) in thymus, mature CD4+ *T*-cells in spleen (CD4+CD3+), mature CD8+ cells in spleen (CD8+CD3+). Tumour burden in *MYC;Dnmt3b*$^{+/+}$ and *MYC;Dnmt3b*$^{Cl/Cl}$ mice was evaluated using CD4+ and CD8+ antibodies. Data were acquired on the LSRFortessa flow cytometers (BD Biosciences, San Diego, CA, USA) and analysed with FACSDiva software (BD Biosciences, San Diego, CA, USA). For quantification of 5mdCs, B-cells (CD19+) from spleen and T-cells (CD4+/CD8+) from thymus were isolated by FACs sorting using FACSAria cell sorter (BD Biosciences, San Diego, CA, USA).

The analysis of clonality in tumours was performed by using Mouse Vβ TCR screening kit (BD PharMingen). Aliquots of cell suspensions isolated from spleens of terminally sick mice were stained with a panel of mAbs recognizing TCR Vβ chain, including Vβ 2, 3, 4, 5.1 and 5.2, 6, 7, 8.1 and 8.2, 8.3, 9, 10b, 11, 12, 13, 14, and 17a TCR per manufacturer's instruction. Tumours were considered monoclonal if they stained for one TCR, biclonal if they stained for two different TCRs, etc.

In vivo BrdU labelling of tumour T-cells in terminally sick mice was performed via i.p. injection of BrdU (100 mg per kg of body weight) 2 h before harvest. Normal thymocytes or thymic tumour cells were stained with anti-CD4-PE and anti-CD8-PerCP, and BrdU-positive cells were quantified using anti-BrdU-FITC (BrdU- Flow Kit, BD Biosciences PharMingen) as described by the manufacturer. For *in vitro* BrdU labelling, BrdU at a concentration of 0.01 mM was added 110 min before harvests of cells.

2.9. WGBS and bioinformatics analysis

The WGBS libraries were prepared and sequenced on an Illumina NovaSeq6000 sequencer using 150 bp long paired-end reads

(Novogene, USA). Publicly available WGBS data for mouse thymus control were obtained from ENCODE (Joe Ecker, Salk lab, ENCSR001MFH) [26]. Quality check, trimming, filtering, and alignment of reads to the *Mus musculus* UCSC mm10 reference genome was performed at the ICBR Bioinformatics Core (UF, Florida). The aligned BAM files were uploaded to the Galaxy web platform [27]. Methylation calling was performed with Methyldackel (v 0.3.0.1) using the mm10-CG index (https://github.com/dpryan79/MethylDackel.git). Only CpG sites with a minimum sequencing depth 5x were included in analysis. Methylation scores were visualized with the Integrated Genome Browser (IGB) [28]. Scatter plots of methylation score were generated in Rstudio v1.1.4.6 using package gplots.

DMRs were determined by Metilene [29] and defined based on average of minimum three consecutive DMCs with methylation change of ≥20% in the same direction with p-values <0.05 (as determined by MWU test). Maximal base pair cut-off for a distance between consecutive DMCs in DMR was set to 50 bp. Annotation of methylated CpGs and DMRs to long promoters, gene bodies, enhancers, and repeats was performed using bedtools intersect. The DMR was retained if the overlap between these elements and DMR was at least 50% of the length of the DMR. Chromosomal coordinates of TSS, gene bodies, and repeats were acquired from the USCS Table browser. Enhancers coordinates identified in CD4+CD8+ cells and thymus cells were obtained from Enhancer atlas [30]. Long promoter was defined as 1500 bp upstream to 500 bp downstream of the TSS.

2.10. Quantification of 5mdCs

Combined liquid chromatography-tandem mass spectrometry with multiple reaction monitoring (LC-MS/MS-MRM) was applied to quantify 5mdCs levels in DNA extracted from sorted T-cells (CD4+CD8+) and B-cells (CD19+) of *Dnmt3b*$^{+/+}$ and *Dnmt3b*$^{CI/CI}$ mice. DNA hydrolysis was performed by using DNA Degradase Plus (Zymo Research). Briefly, 400 ng of genomic DNA was mixed with 2 μl of 10x DNA Degradase Reaction buffer, 1 μl DNA Degradase Plus and water to make a total reaction volume of 20 μl. Finally, the reaction was inactivated with heating to 70 °C for 20 min. Liquid phase chromatography was performed using gradient elution from a 2.1 × 100 mm Hypersil GOLD aQ C18 reversed-phase column with a guard cartridge and an Accela 600 quaternary pump at 250 μl/min at 40 °C. Transition pairs (258.2 → 141.93 *m/z* for 5HmdC, 242.2 → 126.10 *m/z* for 5mdC, and 268.1 → 152.3 *m/z* for dG) were monitored on a Thermo Scientific TSQ Vantage Triple Quadrupole mass spectrometer at dwell times of 0.375 s each and scan widths of 0.002 *m/z*. The collisional gas pressure was set at 1.2mTorr. The raw data were analysed with the Xcalibur Qual Browser using ICIS peak detection with following parameters: baseline windows of 30 units for 5mdC and 5HmdC, windows of 40 units for dG, the minimum signal-to-noise ratio 3.0, and the peak detection set for the highest peak option. Concentrations of 5mdC were calculated as a percentage of 2′-deoxyguanosine (dG). The calibrated ranges for the samples were 0–25% for 5mdC using a fixed 40 pmol amount of dG as an internal standard. Replicates for the unknown samples were run in triplicate followed by a blank to eliminate carryover into the next unknown run. All the procedures were carried out by Zymo Research Epigenetic Services (Zymo Research Corp, CA, USA).

2.11. Real-time qRT-PCR

RNAs were reverse transcribed with the SuperScript III Reverese transcriptase (Thermo Fisher) using oligo(dT) primers. Real-time qRT-PCR was performed with the iQ™ SYBR® Green Supermix (Bio-Rad) on a CFX96 Touch™ Real-Time PCR Detection System (Bio-Rad). Fast PCR cycling conditions were used (95 °C for 3 min, 40 cycles (95 °C for 10 s, 58–63.5 °C for 30 s)), followed by a dissociation curve analysis. All qPCR measurements were performed in duplicate reactions and normalized to the expression of housekeeping gene (*β-actin*). In parallel, no-RT controls were amplified to rule out the presence of contaminating genomic DNA. Primer sequences for qPCR are provided in Supplementary Data 5.

2.12. RNA-seq

Library generation and sequencing was performed on NovaSeq 6000 platform using paired-end 150 bp runs (Novogene, USA). Tissue samples from seven Peripheral T-cell lymphomas were provided by the NCI Cooperative Human Tissue Network (CHTN). Other investigators may have received samples from the same tissue specimens. Three total RNA samples isolated from PTCL tumours were acquired from Origene (Rockville, MD, USA). The Institutional Review Board of the University of Nebraska Medical centre approved the use of these samples. Sample description is summarized in Supplementary Data 3.

Publicly available RNA-seq data for thymus of *Dnmt3b*$^{+/+}$ mice were obtained from GEO (GSE109255). Publicly available data for human T-cell lymphoma tumours were obtained from GEO (GSE109231, GSE143986, GSE111320, GSE57944) and SRA (SRP044708, SRP049695, SRP099016). Publicly available data on human normal T-cell controls were downloaded from GEO (GSM1060237 and GSM1060238). Trimmed sequencing data were first aligned to *M. musculus* UCSC mm10 or to *Homo sapiens* UCSC hg19 reference genome using STAR aligner. RNA-seq data with minimum mapped quality 50 were quantified using the RNA-seq quantification pipeline in SeqMonk software (http://www.bioinformatics.babraham.ac.uk/projects/seqmonk/). DESeq2 was used to calculate differential expression. For differentially expressed genes, only genes with a fold change ≥2 and a p value <0.05 were considered to be significant. KEGG pathway analysis was conducted using WebGestalt. Ingenuity pathway analysis (Qiagen) [31] was used to analyse activated and decreased signalling pathways. The transcriptome data projection in 2D by t-SNE was generated using HEMAP [32].

2.13. Gene set enrichment analysis (GSEA)

All FPKM values for *MYC;Dnmt3b*$^{+/+}$, *MYC;Dnmt3b*$^{CI/CI}$ tumours and control thymus were converted to GCT expression dataset. CLS files were generated using CLSFileCreator (v4) (http://software.broadinstitute.org/cancer/software/genepattern/modules/docs/ClsFileCreator/4). Curated gene set was downloaded from Broad Institute's Molecular Signatures Database. Gene Set Enrichment Analysis (v3.0) was used to test the relationship between RNA-seq expression data and the Curated gene set. Gene sets enriched in less than 15 genes and more than 500 genes were excluded from the analysis. Gene sets with a false discovery rate (FDR) value <0.25 and p <0.05 after performing 1000 permutations were considered to be significantly enriched.

2.14. Statistical analysis

Statistical significance of means ±SEM was evaluated using the two-tailed Student's *t*-test. For all statistical analyses p values <0.05 were considered significant. The significance between observed and expected genotype representation of Dnmt3b$^{+/CI}$ and Dnmt3b$^{CI/CI}$ mice was calculated using Chi-squared test. Differential histone enrichment was analysed by Student's *t*-test or Welch's unequal variances *t*-test with threshold of p value <0.05.

2.15. Role of the funding source

Funders were not involved in study design, data collection, data analyses, interpretation or writing the report.

3. Results

3.1. Dnmt3b$^{CI/CI}$ mice survive postnatal development but develop ICF-like syndrome

We have previously reported a generation of *Dnmt3b^{CI}* allele expressing catalytically inactive Dnmt3b from endogenous locus [13]. This allele has a two amino acid (aa) substitution in active site of Dnmt3b rendering protein catalytically inactive (Fig. 1a). Unlike *Dnmt3b$^{-/-}$* mice, *Dnmt3b$^{CI/CI}$* mice survived embryogenesis [13]. While *Dnmt3b$^{+/CI}$* mice were like their *wild-type* littermates, *Dnmt3b$^{CI/CI}$* mice presented with ~20% decrease in body weight at weaning and this difference persisted throughout their postnatal lives (Fig. 1b, c). Despite decreased size, both *Dnmt3b$^{CI/CI}$* males and

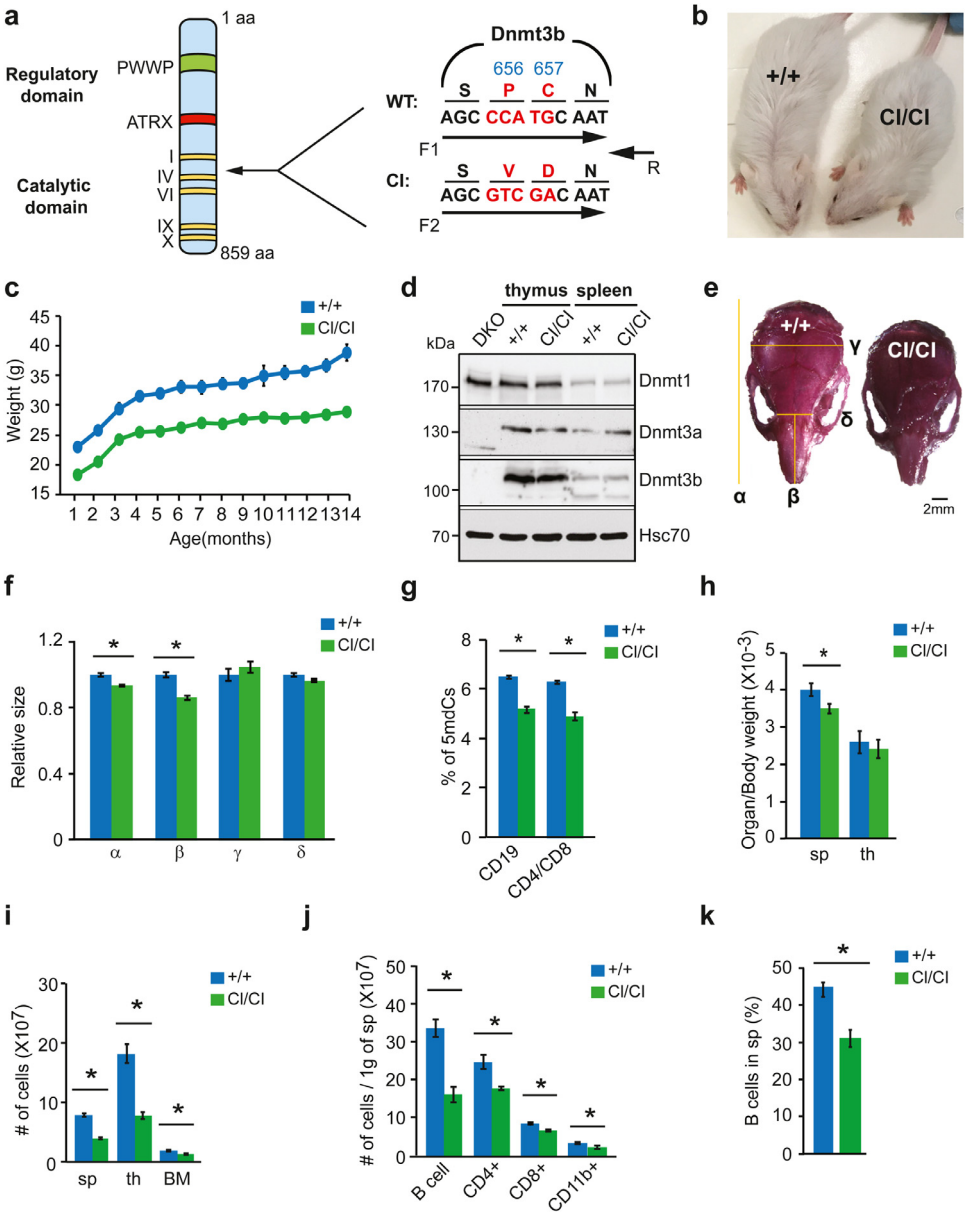

Fig. 1. Mice expressing catalytically inactive Dnmt3b develop ICF-like phenotype.

a. *(left)* Schematic representation of mouse Dnmt3b protein structure. Regulatory domain containing PWWP and ATRX domains and catalytic domain with methyltransferase motifs (I, IV, VI, IX and X) are depicted *(right)*. Nucleotide and amino acid sequences of exon 19 in *wild-type* (WT) and *Dnmt3b^{CI}* (CI) allele. Amino acid substitution (P656V and C657D) in CI allele results in inactivation of the CA [13]. Position of genotyping primers is indicated by arrows. F1-R detects *wild-type* sequence; F2-R detects mutated sequence. b. Micrograph of 6-week-old *Dnmt3b$^{+/+}$* (+/+) and *Dnmt3b$^{CI/CI}$* (CI/CI) mice. c. Body weight values of *Dnmt3b$^{+/+}$* and *Dnmt3b$^{CI/CI}$* mice at indicated ages ($n = 10$). $p<0.05$ by two-tailed Student's *t*-test. d. Immunoblot of Dnmt1, Dnmt3a and Dnmt3b expression in spleen and thymus of 8-weeks old *Dnmt3b$^{+/+}$* and *Dnmt3b$^{CI/CI}$* mice. *Dnmt3a$^{-/-}$;Dnmt3b$^{-/-}$* mouse T-cell lymphoma line (DKO) served as negative control. Hsc70 served as a loading control. e. Gross morphology of skulls of *Dnmt3b$^{+/+}$* and *Dnmt3b$^{CI/CI}$* mice. Scale bar represents 2 mm. f. Dimensions of skulls of *Dnmt3b$^{+/+}$* (blue, $n = 3$) and *Dnmt3b$^{CI/CI}$* (green, $n = 4$) mice. Orientation of α, β, γ and δ dimensions is depicted by orange lines on the image in (e). $^*p = 0.005$ for α; $p = 0.003$ for β. g. Percentage of 5-methyl-deoxy-cytidines (5mdCs) in DNA of FACS-sorted splenic B-cells (CD19+) and thymocytes (CD4+CD8+) isolated from *Dnmt3b$^{+/+}$* (blue, $n = 3$) and *Dnmt3b$^{CI/CI}$* (green, $n = 3$) mice as determined by mass spectrometry. $^*p<0.01$. h. Weights of spleen (sp) and thymus (th) of *Dnmt3b$^{+/+}$* (blue, $n = 23$) and *Dnmt3b$^{CI/CI}$* (green, $n = 24$) mice and normalized to body weight. $^*p = 0.024$. i. Absolute cell counts in spleen ($n = 8$), thymus ($n = 7$) and bone marrow (BM, $n = 8$) in *Dnmt3b$^{+/+}$* (blue) and *Dnmt3b$^{CI/CI}$* (green) mice. $^*p<0.05$. j. Cell counts normalized to spleen weight of B-cells (CD19+B220+), mature T-cells (CD4+CD3+ and CD8+CD3+) and myeloid cells (CD11b+CD5-) in spleen of *Dnmt3b$^{+/+}$* (blue) and *Dnmt3b$^{CI/CI}$* (green) mice ($n = 6$). $^*p<0.05$. k. Percentage of total B-cells in spleen of FVB recipient mice reconstituted with BM of *Dnmt3b$^{+/+}$* (blue) and *Dnmt3b$^{CI/CI}$* (green) mice ($n = 5$). $^*p = 0.0029$.

All the data in figure are presented as mean ± SEM, p-value was calculated by two-tailed Student's *t*-test.

females had normal lifespan. Dnmt3b^{CI} levels were similar to Dnmt3b^{WT} levels in adult thymus and spleen demonstrating that the amino acid substitutions did not adversely affect Dnmt3b regulation (Fig. 1d). The levels of DNA methyltransferases Dnmt1 or Dnmt3a did not seem to be affected by replacement of Dnmt3b^{WT} for Dnmt3b^{CI} either, at least in the tested tissues (Fig. 1d).

A closer examination of *Dnmt3b$^{CI/CI}$* mice revealed craniofacial defects including shortened nose (Fig. 1e, f). The axial length of *Dnmt3b$^{CI/CI}$* calvarium was significantly shorter, whereas the width of the parietal bones was similar as that of the control mice.

These features are similar to the hypertelorism and the flat nasal bridge frequently seen in individuals with ICF syndrome [33]. Global 5-methylcytosine levels in DNA from *Dnmt3b$^{CI/CI}$* B- and T-cells was reduced (Fig. 1g), consistently with observation in human ICF patients [34]. Sizes of thymi and spleens in *Dnmt3b$^{CI/CI}$* mice were slightly decreased even after normalization to the body weight with concomitant 20−50% reduction in the cellularity that could also be seen in bone marrow (BM) (Fig. 1h, i). The number and percentages of T- (CD3+ CD4+ and CD3+ CD8+), myeloid (CD11b+) and in particular B-cells (CD19+B220+) were significantly decreased in spleens of *Dnmt3b$^{CI/CI}$* mice (Figs. 1j and S1a). Inefficient B-cell lymphopoiesis was already seen in BM manifested by a reduction in immature B-cells, pre-pro- and pro- B-cells in BM and affected both mature and transitional B-cells in spleen (Figure S1b, c and data not shown).

Similarly but to a lesser extent, thymopoiesis was decreased as shown by a reduction in number of CD4-CD8- double-negative (DN1−4) populations, CD4+CD8+ double positive (DP) and single positive CD4+ and CD8+ in thymus of *Dnmt3b$^{CI/CI}$* mice accompanied by a reduction in mature T-cells (CD4+CD3+; CD8+CD3+) in spleens (Figure S1d-g). Less efficient haematopoiesis is at least partially attributable to a reduction in number of Lin-c-kit+Sca-1+ (LSK) in *Dnmt3b$^{CI/CI}$* BM which is a compartment that harbours haematopoietic stem cells (Figure S2a, b). B-cell defects are autonomous to haematopoietic system because analysis of recipient mice reconstituted with *Dnmt3b$^{CI/CI}$* BM produced this lineage less efficiently whereas T-cell and myeloid lineages were unaffected (Figs. 1k, S2c, d and data not shown).

Altogether, our data indicate that loss of Dnmt3b's CA induces phenotypes consistent with ICF syndrome in humans, in particular craniofacial defects, a decreased body weight, global DNA hypomethylation and less efficient adult haematopoiesis with a decreased production of all lineages and B-cells in particular. Thus, Dnmt3b's CA is critical to prevent ICF-like syndrome in mice.

3.2. *Loss of* Dnmt3b's *CA promotes cellular transformation in vitro and in vivo*

Loss of Dnmt3b sensitizes primary mouse embryonic fibroblasts (MEFs) to spontaneous immortalization thereby likely promoting cellular transformation [35]. To analyse the role of Dnmt3b's CA, we next utilized primary MEFs derived from E13.5 *Dnmt3b$^{+/+}$* and *Dnmt3b$^{CI/CI}$* embryos to test effects of the genetic background on cellular growth. We did not observe any differences between normal MEFs of these two genotypes in ability to generate sparse, diffused colonies in limited dilution experiments or in overall ability to grow *in vitro* (Fig. 2a- d). To test the role of Dnmt3b's CA in fibroblast transformation, we next ectopically expressed exogenous c-Myc along with the activated form of *Ras* (*H-Ras^{V12}*) that are known to induce transformation upon concomitant expression in primary MEFs [36]. Early passages of MEFs were transduced with retroviral vectors expressing *Myc* and *Ras* and co-expressing Red Fluorescent Protein (RFP) and Green Fluorescent Protein (GFP), respectively. Transduction efficiency was >95% as determined by FACS analysis of RFP and EGFP expression (Figure S3a). RFP+EGFP+ expressing MEFs of both genotypes quickly underwent cellular transformation manifested morphologically by elongated shape and loss of contact inhibition (Fig. 2b). Consistently, transformed cells expressed increased levels of Myc and Ras (Fig. 2e). Interestingly, the transformed *Dnmt3b$^{CI/CI}$* MEFs formed ~3 fold more colonies than *wild-type* counterparts and proliferated at increased levels suggesting that loss of Dnmt3b's CA promotes fibroblast transformation *in vitro* (Fig. 2b-d). The increased ability of transformed *Dnmt3b$^{CI/CI}$* to grow and form colonies relative to *Dnmt3b$^{+/+}$* was confirmed by independent MEFs lines isolated from different embryos of the same genotypes (Figure S3b-d). To elucidate its role further, we next re-introduced catalytic activity into *Dnmt3b$^{CI/CI}$* MEFs by ectopic expression of *wild-type* Dnmt3b and subsequently induced transformation of these cells by transduction with retroviruses expressing *Myc* and *Ras*. Analysis of these cells revealed successful expression of w*ild-type* Dnmt3b (Fig. 2f) and decreased ability of cells to form colonies and grow relative to that the Myc/Ras transformed *Dnmt3b$^{CI/CI}$* MEFs further supporting the idea that Dnmt3b's CA is important to suppress cellular transformation. Reintroduction of Dnmt3b, however, did not fully decreased growth properties of transformed *Dnmt3b$^{CI/CI}$* MEFs to the levels observed in transformed *Dnmt3b$^{+/+}$* MEFs presumably because *de novo* activity of Dnmt3b upon reintroduction into cells is unable to restore all methylation defects these cells may have acquired during embryogenesis and/or *in vitro* growth.

To further assess tumourigenicity, transformed *Dnmt3b$^{+/+}$*and *Dnmt3b$^{CI/CI}$* MEFs were injected subcutaneously into nude mice. By one month, mice had to be sacrificed, as all of the injected sites contained rapidly growing tumours. Mean tumour weights derived from *Dnmt3b$^{CI/CI}$* MEFs were ~3-fold larger relative to *wild-type* counterparts (Fig. 2g, h). Thus, Dnmt3b's CA suppresses MEFs transformation *in vitro* and growth of transformed cells *in vivo*.

To further test the relevance of Dnmt3b's CA in tumourigenesis, we utilized a model of Acute Myeloid Leukaemia (AML) induced by MLL-AF9 overexpression in BM cells followed by transplantation into lethally irradiated recipients in which Dnmt3b elimination was shown to accelerate disease initiation and progression [25]. We first transduced *Dnmt3b$^{+/+}$* and *Dnmt3b$^{CI/CI}$* BM cells with a retroviral *MLL-AF9* fusion gene in IRES with EGFP. Equal number of *Dnmt3b$^{+/+}$* and *Dnmt3b$^{CI/CI}$* EGFP-positive cells was mixed with untransduced *Dnmt3b$^{+/+}$* BM cells and transplanted into lethally irradiated FVB recipients to generate cohorts of mice with *Dnmt3b$^{+/+}$* and *Dnmt3b$^{CI/CI}$* haematopoietic system expressing driver of AML and EGFP. Both groups of mice developed immunophenotypically same AML (CD11b+, Gr-1+) but mice injected with MLL-AF9 *Dnmt3b$^{CI/CI}$* cells developed the disease significantly faster than control mice (Median survival (MS) of 63 days *versus* MS=74) (Fig. 2i, j). These data suggest that Dnmt3b's CA plays a role in its TS function in MLL-AF9-induced AML.

3.3. *Dnmt3b's CA is critical for its tumour suppressor function in MTCL*

To determine if Dnmt3b's CA is important for its TS function in mouse MTCL [21], we compared survival in cohorts of *Eμ*SR*α-tTA; Teto-MYC;Dnmt3b$^{+/+}$* (termed *MYC;Dnmt3b$^{+/+}$*) and *Eμ*SR*α-tTA;Teto-MYC;Dnmt3b$^{CI/CI}$* (*MYC;Dnmt3b$^{CI/CI}$*) mice (Figure S4a). Consistently with our previous results, MS of control *MYC;Dnmt3b$^{+/+}$*mice was 94 days (Fig. 3a) [11,21,37]. Lymphomagenesis was accelerated in *MYC;Dnmt3b$^{+/CI}$* mice and even more significantly in *MYC;Dnmt3b$^{CI/CI}$* mice that developed lymphomas very quickly and died with MS of 27 days (Fig. 3a). Like *MYC;Dnmt3b$^{+/+}$* mice, *MYC;Dnmt3b$^{CI/CI}$* developed either CD4+CD8+ or CD4+ lymphomas and this immunopthentypic spectrum was similar between both groups (Figs. 3b and S4b). Importantly, lymphomas from both groups were serially transplantable upon intraperitoneal (IP) injection into *wild-type* recipient mice demonstrating their true malignant potential (Fig. 3b). *MYC; Dnmt3b$^{CI/CI}$* lymphoma grew faster as indicated by higher proliferative indices (Figure S4c). Lymphomas of both groups were likely monoclonal as indicated by uniform expression of TCR receptors in all cells of individual tumours (Figs. 3c and S4d). MYC, Dnmt3b and

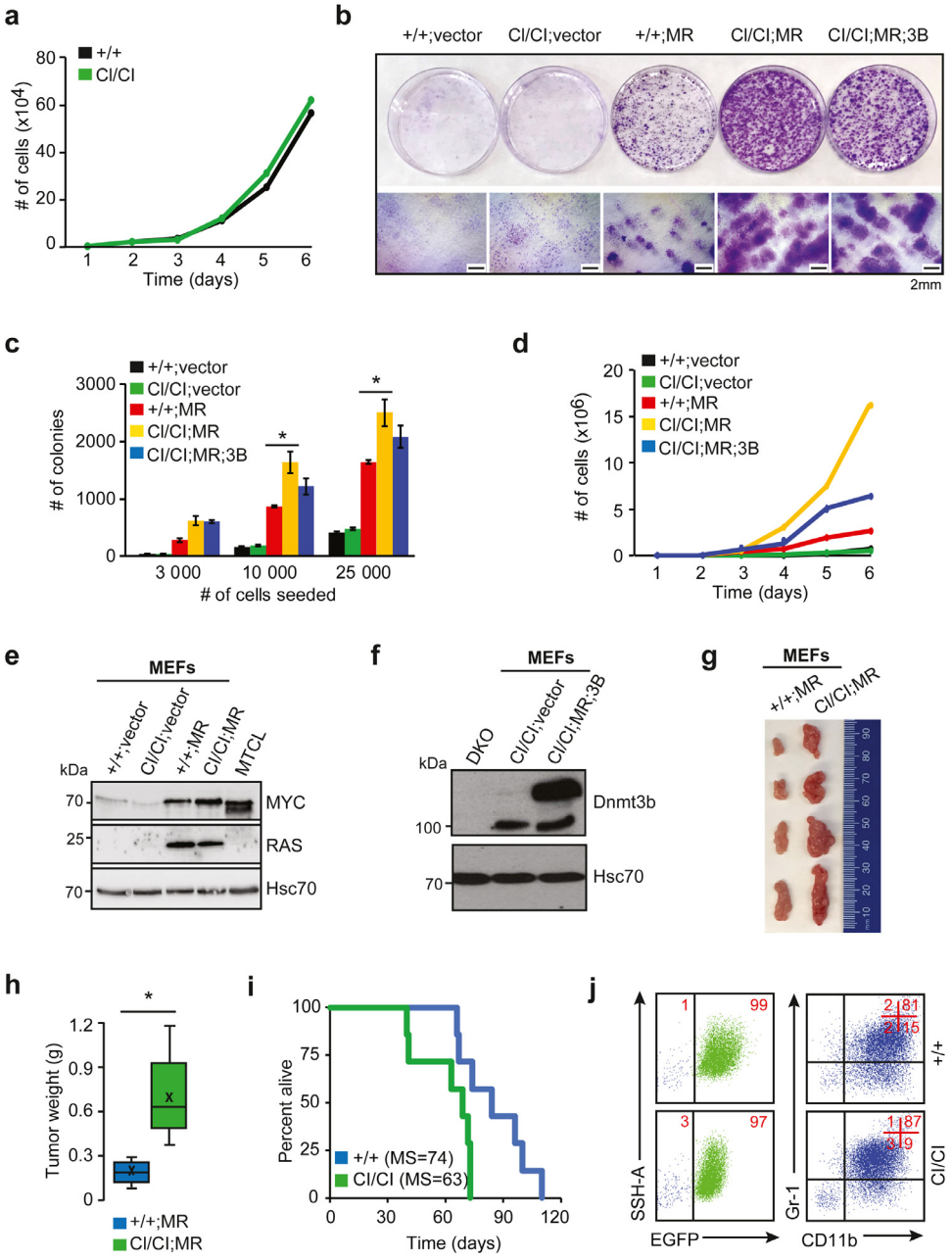

Fig. 2. Loss of Dnmt3b's CA promotes cellular transformation *in vitro* and *in vivo.*

a. Proliferation rate of $Dnmt3b^{+/+}$ (+/+) and $Dnmt3b^{CI/CI}$ (CI/CI) MEFs cells. Representative results of one out of three experiments are shown. b. Colony formation assay of $Dnmt3b^{+/+}$ and $Dnmt3b^{CI/CI}$ MEFs cells transduced with lentiviral control vector (+/+;vector and CI/CI;vector, respectively), MEFs transformed with vectors expressing c-Myc and Ras (+/+;MR and CI/CI;MR) and transformed $Dnmt3b^{CI/CI}$ MEFs transduced with lentiviral vector encoding $Dnmt3b^{WT}$ (CI/CI;MR;3B). Top pictures depicts culture plates with macroscopically visible colonies after fixation and crystal violet staining. Lower pictures show the same colonies at the microscopic level (8x magnification). Scale bar represents 2 mm. c. Quantification of number of colonies obtained from experiment described in (b). Cells were seeded at depicted numbers. Data are presented as mean ±SEM from three independent experiments. $^{*}p<0.05$ by two-tailed Student's *t*-test. d. Proliferation rate of cells used in experiment described in (b). Representative results of one out of three experiments are shown. e. Immunoblot of Myc and Ras expression in untransformed and transformed $Dnmt3b^{+/+}$ and $Dnmt3b^{CI/CI}$ MEFs cells. $Dnmt3a^{-/-};Dnmt3b^{-/-}$ (DKO) line served as negative control. Mouse MYC-induced T-cell lymphoma line (MTCL) served as positive control. Hsc70 served as a loading control. f. Immunoblot of Dnmt3b expression in $Dnmt3b^{CI/CI}$ MEFs transduced with control vector (CI/CI;vector) and transformed $Dnmt3b^{CI/CI}$ MEFs transduced with vector encoding FLAG-tagged $Dnmt3b^{WT}$ (CI/CI;MR;3B). $Dnmt3a^{-/-};Dnmt3b^{-/-}$ (DKO) line served as negative control. Hsc70 served as a loading control. g. Micrographs of tumours isolated from nude mice injected with transformed $Dnmt3b^{+/+}$ and $Dnmt3b^{CI/CI}$ MEFs. h. Weights of tumours derived from transformed $Dnmt3b^{+/+}$ and $Dnmt3b^{CI/CI}$ MEFs grown in nude mice ($n = 6$). Horizontal line represents median, bounds of box-likely range of variation and whiskers-min and max values $^{*}p = 0.0158$ by two-tailed Student's *t*-test. i. Kaplan Meier (KM) survival curves of lethally irradiated FVB recipient mice reconstituted with $Dnmt3b^{+/+}$ or $Dnmt3b^{CI/CI}$ ($n = 7$, each) BM cells transduced with retrovirus encoding MLL-AF9. Median survival (MS) is indicated. $p = 0.044$ by log rank test. j. EGFP, Gr-1 and CD11b expression in cells isolated from BM of terminally sick recipient mice reconstituted with $Dnmt3b^{+/+}$ or $Dnmt3b^{CI/CI}$ transduced with MLL-AF9. The percentage of positive cells is indicated within the FACS diagrams.

Dnmt3a were expressed similarly in *MYC;*$Dnmt3b^{+/+}$ and *MYC;*$Dnmt3b^{CI/CI}$ lymphomas suggesting that differences in lymphomagenesis were not due to effects of $Dnmt3b^{CI}$ protein on transgenic *MYC* or other Dnmts (Fig. 3d, e). Tumours that developed in lethally irradiated recipient mice whose haematopoietic system was reconstituted with *MYC;*$Dnmt3b^{CI/CI}$ foetal liver cells were clonal and lymphomagenesis was accelerated suggesting that the effects of Dnmt3b's CA on lymphomagenesis are autonomous to haematopoietic system and are not just a function of reduced body size of $Dnmt3b^{CI/CI}$ mice (Figs. 3f, g and S4e, f).

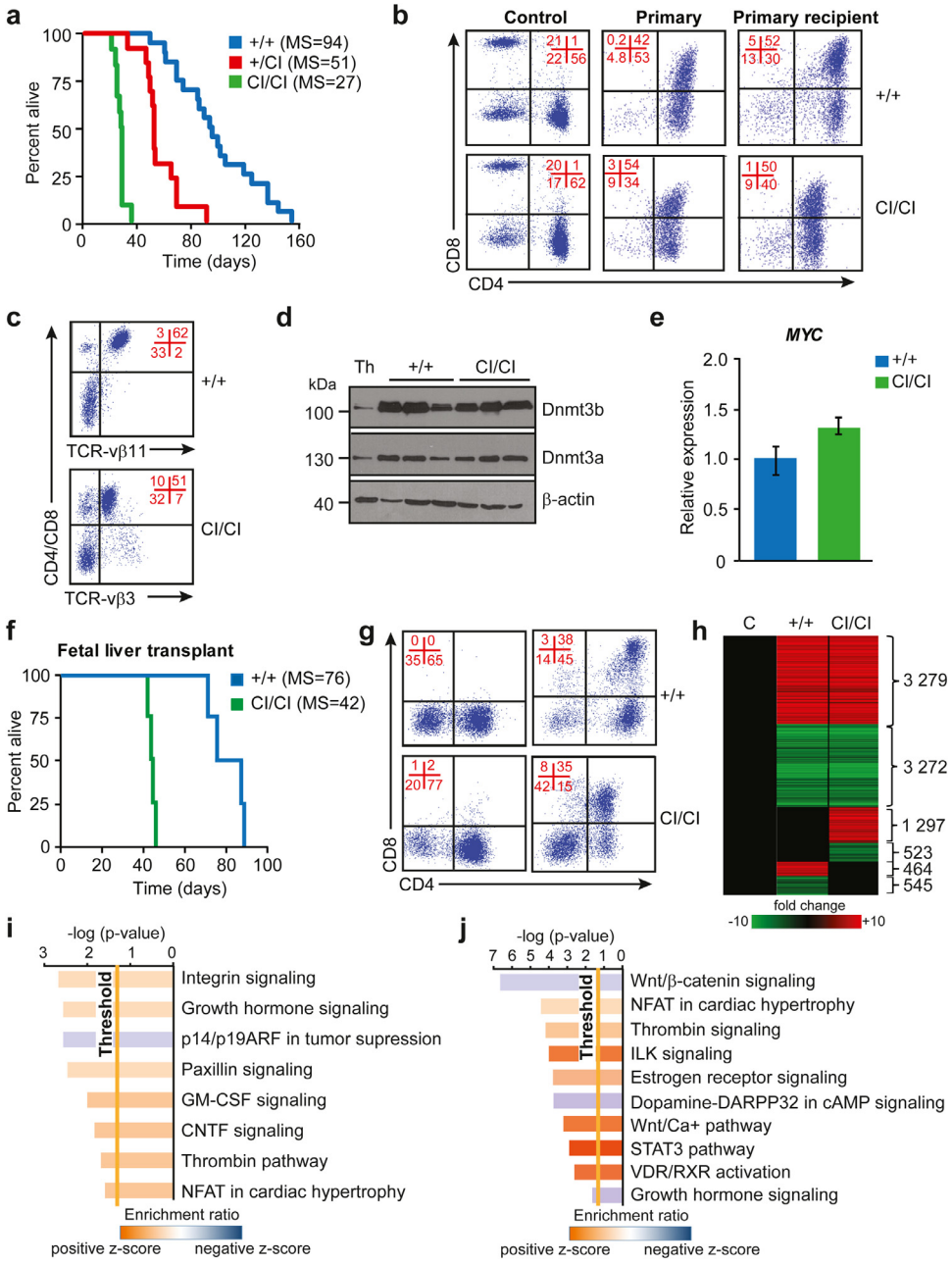

Fig. 3. Loss of Dnmt3b's CA accelerates MYC induced lymphomagenesis.

a. KM survival curve of *MYC;Dnmt3b*$^{+/+}$ (+/+, n = 20), *MYC;Dnmt3b*$^{+/CI}$ (+/CI, n = 13) and *MYC;Dnmt3b*$^{CI/CI}$ (CI/CI, n = 12) mice. $p<0.001$ by log rank test. b. CD4 and CD8 expression in cells isolated from lymph nodes (LN) of healthy *Dnmt3b*$^{+/+}$ mice (Control), terminally sick *MYC;Dnmt3b*$^{+/+}$ and *MYC;Dnmt3b*$^{CI/CI}$ mice (Primary) as analysed by FACS. Analysis of tumour that developed in sublethally irradiated FVB recipient mice (Primary recipient) injected with primary tumour cells is also shown. c. FACS diagram showing clonal TCR-vβ expression in a *MYC;Dnmt3b*$^{+/+}$ and *MYC;Dnmt3b*$^{CI/CI}$ tumour.

d. Immunoblot of Dnmt3b and Dnmt3a protein levels in healthy thymus (Th), *MYC;Dnmt3b*$^{+/+}$and *MYC;Dnmt3b*$^{CI/CI}$ lymphomas. β-actin served as a loading control.

e. Relative FPKM expression values of human *MYC* transgene in *MYC;Dnmt3b*$^{CI/CI}$ (n = 5) lymphomas compared to *MYC;Dnmt3b*$^{+/+}$ (n = 3) lymphomas as determined by RNA-seq. f. KM survival curves of lethally irradiated FVB recipient mice reconstituted with foetal liver of E15.5 *MYC;Dnmt3b*$^{+/+}$ (n = 4) and *MYC;Dnmt3b*$^{CI/CI}$ (n = 4) embryos. p = 0.0067 by log rank test. g. CD4 and CD8 expression in lymphomas developed in lethally irradiated FVB recipient mice injected with foetal liver of E15.5 *MYC;Dnmt3b*$^{+/+}$ or *MYC;Dnmt3b*$^{CI/CI}$ embryos. h. Heat map showing fold change expression values of subset of differentially expressed genes (FC≥3, $p<0.05$ by DESeq) in *MYC;Dnmt3b*$^{+/+}$ (n = 3) and *MYC;Dnmt3b*$^{CI/CI}$ lymphomas (n = 5) when compared to control T-cells (C, n = 3). i. Ingenuity Pathway Analysis (IPA) of genes differentially expressed (FC≥3, $p<0.05$ by DESeq) in *MYC;Dnmt3b*$^{+/+}$but not in *MYC;Dnmt3b*$^{CI/CI}$ lymphomas. The top canonical pathways are displayed ($p<0.05$ by right-tailed Fisher's exact test). j. IPA of genes differentially expressed (FC≥3, $p<0.05$ by DESeq) in *MYC;Dnmt3b*$^{CI/CI}$ but not in *MYC;Dnmt3b*$^{+/+}$lymphomas. The top canonical pathways are displayed ($p<0.05$ by right-tailed Fisher's exact test).

Analysis of global gene expression patterns obtained from lymphomas and control cells by RNA-seq revealed that a majority of deregulated genes (~9000; FC≥3; $p<0.05$ by DESeq) were shared between *MYC;Dnmt3b*$^{+/+}$ and *MYC;Dnmt3b*$^{CI/CI}$ lymphomas, with around 3000 genes specific to both groups (Figs. 3h and Supplementary Data 1). Ingenuity Pathway Analysis (IPA) revealed similarly deregulated signalling with shared deregulated pathways such as *Thrombin* and *NFAT signalling* (Fig. 3i, j). Some pathways such as *STAT3, Wnt/Ca+* and *ILK signalling* were upregulated only in *MYC;Dnmt3b*$^{CI/CI}$ lymphomas. Altogether, these results suggest that Dnmt3b's CA is critical for its TS function in MTCL, operates within haematopoietic system and may be linked to various signalling pathways including STAT3 signalling.

3.4. Dnmt3b's AF suppresses genome-wide hypomethylation in lymphomagenesis

To address the effects of Dnmt3b on tumour methylome, we next analysed global DNA methylation patterns in *MYC;Dnmt3b*$^{+/+}$, *MYC;Dnmt3b*$^{CI/CI}$ and previously generated *EμSRα-tTA;Teto-MYC;Teto-Cre;Rosa26LOXP*^{EGFP}*;Dnmt3b*$^{fl/fl}$ (termed *MYC;Dnmt3b*$^{Δ/Δ}$) lymphomas [21]. Whole Genome Bisulfite sequencing yielded methylation readout on ~1.4 × 10^7 million CGs (coverage ≥5x), out of which >1.1 × 10^7 CGs present in all samples were compared to data on normal thymus (ENCSR001MFH) [26] (Table S1).

All tumours were characterized by genome-wide hypomethylation with the highest percentage of hypomethylated cytosines (19%) in *MYC;Dnmt3b*$^{Δ/Δ}$ lymphomas (Figs. 4a, b and S5a, b). In contrast, <1% of CGs gained methylation in lymphomas (Figs. 4b and S5b). Similarly, 10 times more hypo- than hypermethylated differentially methylated regions (DMRs) were seen in tumours in various genome areas (Fig. 4c). A portion of hypo- and hypermethylated DMRs were shared in lymphomas likely generated independently of Dnmt3b functions (Fig. 4d).

To understand effects of Dnmt3b's CA and AF on methylome, we next analysed methylation changes detected specifically in *MYC;Dnmt3b*$^{Δ/Δ}$ and *MYC;Dnmt3b*$^{CI/CI}$ lymphomas. A majority of hypomethylated DMRs in *MYC;Dnmt3b*$^{Δ/Δ}$ lymphomas were not detected in *MYC;Dnmt3b*$^{CI/CI}$ lymphomas suggesting that Dnmt3b's AF may have participated in their methylation (Fig. 4e). Around 6000 DMRs were seen hypomethylated in both setting suggesting that these are targets of Dnmt3b's CA.

Thus, Dnmt3b's AF may be less effective in contributing to integrity of tumour methylome, compared to embryogenesis where it rescued 90% of methylation at E11.5 [13].

The fact that 28140 DMRs hypomethylated in *MYC;Dnmt3b*$^{Δ/Δ}$ lymphomas are not affected in *MYC;Dnmt3b*$^{+/+}$ and *MYC;Dnmt3b*$^{CI/CI}$ lymphomas (Fig. 4e) indicates that Dnmt3b^{CI} protein is sufficient for their methylation. Thus, these loci may be putative targets of Dnmt3b's AF, *e.g. Dhcr24* locus, and we term them *catalytic-independent DMRs* (Fig. 4f). In contrast, 6785 loci were hypomethylated in both *MYC;Dnmt3b*$^{Δ/Δ}$ and *MYC;Dnmt3b*$^{CI/CI}$ lymphomas, suggesting that their methylation may depend on Dnmt3b's CA, *e.g. Ankrd36* (Fig. 4e, f) termed *catalytic-dependant* DMRs.

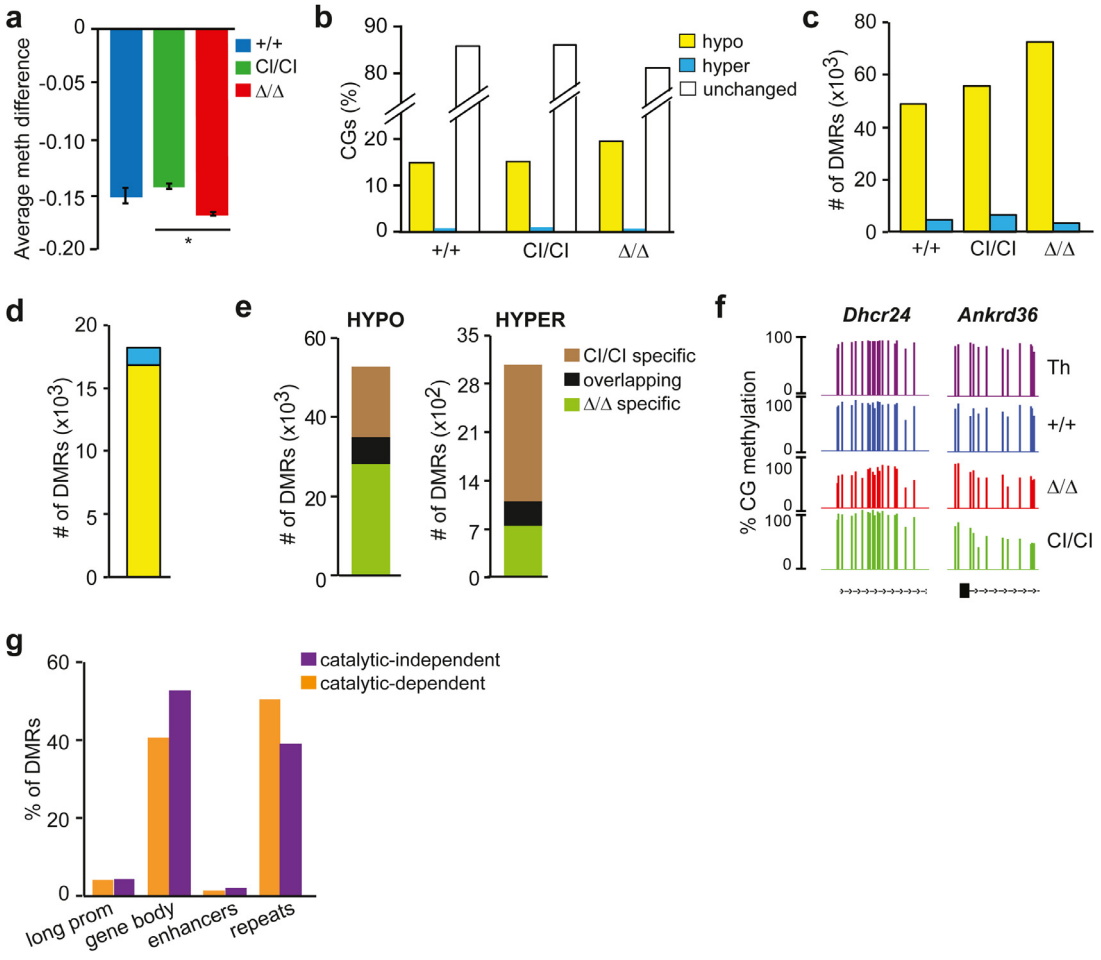

Fig. 4. Association of Dnmt3b functions with methylation and gene expression in mouse T-cells.

a. Comparison of average methylation differences between corresponding CGs of healthy thymus and *MYC;Dnmt3b*$^{+/+}$, *MYC;Dnmt3b*$^{CI/CI}$ and *MYC;Dnmt3b*$^{Δ/Δ}$ lymphomas (n = 2 each). Data are presented as mean ±SEM. *p = 0.0004 by two-tailed Student's t-test. b. Percentages of hypomethylated (yellow), hypermethylated (blue) and unchanged (white) CGs in *MYC;Dnmt3b*$^{+/+}$, *MYC;Dnmt3b*$^{CI/CI}$ and *MYC;Dnmt3b*$^{Δ/Δ}$ lymphomas when compared to healthy thymus (meth. diff. ≥20%). c. Total numbers of hypomethylated and hypermethylated DMRs in *MYC;Dnmt3b*$^{+/+}$, *MYC;Dnmt3b*$^{CI/CI}$ and *MYC;Dnmt3b*$^{Δ/Δ}$ lymphomas relative to healthy thymus (DMRs are regions with methylation difference ≥20% in the same direction in ≥3 consecutive DMCs separated by <50 bp; p(MWU) <0.05). d. Total number of hypomethylated (yellow) and hypermethylated (blue) DMRs identified in all three, *MYC;Dnmt3b*$^{+/+}$, *MYC;Dnmt3b*$^{CI/CI}$ and *MYC;Dnmt3b*$^{Δ/Δ}$ lymphomas relative to healthy thymus (meth. diff. ≥20%; p(MWU) <0.05). e. Total numbers of hypomethylated and hypermethylated DMRs identified only in *MYC;Dnmt3b*$^{CI/CI}$ lymphomas (CI/CI specific), only in *MYC;Dnmt3b*$^{Δ/Δ}$ (*Δ/Δ* specific) and in both *MYC;Dnmt3b*$^{CI/CI}$ and *MYC; Dnmt3b*$^{Δ/Δ}$ lymphomas (overlapping) (meth. diff. ≥20%; p(MWU) <0.05). f. Visualization of single-CG profiles at locus of *Dhcr24* (*catalytic-independent* DMR) and *Ankrd36* (*catalytic-dependant* DMR) in healthy thymus (Th) and *MYC;Dnmt3b*$^{+/+}$, *MYC;Dnmt3b*$^{Δ/Δ}$ and *MYC;Dnmt3b*$^{CI/CI}$ lymphomas. g. Distribution of *catalytic-independent* and *catalytic-dependant* DMRs across indicated genomic regions.

Both *catalytic-dependant* and *catalytic-independent*' DMRs were distributed across the genome with around 4% found in gene promoters (Fig. 4g). About 53% of putative targets of Dnmt3b's AF were found in gene bodies (Fig. 4g). The significance of these putative targets and their interplay with histone marks needs investigated in future studies.

3.5. *c-Met oncogenic pathway is upregulated in* Dnmt3b$^{Cl/Cl}$ *lymphomas*

To understand molecular mechanism underlying an accelerated MTCL in *MYC;Dnmt3b*$^{Cl/Cl}$ linked to Dnmt3b's CA, we next searched for genes with changed methylation and expression. We identified a group of 48 genes specifically hypomethylated and overexpressed in *MYC;Dnmt3b*$^{Cl/Cl}$ lymphomas termed here *Dnmt3b's catalytic signature* (Figs. 5a and Supplementary Data 2). Analysis of this signature identified, amongst others, oncogenic *MAPK, Ras, PI3K-Akt signalling* pathways (Fig. 5b). A unifying feature of the deregulated signalling was c-*Met*-proto-oncogene, a receptor tyrosine kinase [38] enriched in the most pathways, and also detected by GSEA analysis in category '*Met activates PTK2 signalling*' (Fig. 5c). Subsequently, we found that c-Met RNA and protein levels were elevated in *MYC;Dnmt3b*$^{Cl/Cl}$ lymphomas (Fig. 5d, e). The hypomethylated DMRs were observed in promoter (−879 to −823 bp relative to TSS), intron 1 and 17 of *c-Met* specifically in *MYC;Dnmt3b*$^{Cl/Cl}$ lymphomas (Fig. 5f). Because a dysfunctional HGF/c-Met axis is involved in the development of solid tumours affecting pathways including STAT3 signalling [39-41], we next analysed mouse lymphomas and found a specific increase in Stat3 phosphorylation in primary *MYC;Dnmt3b*$^{Cl/Cl}$ malignancies (Fig. 5g). Likewise, a downstream target of Stat3 - RNA binding protein Lin28b [42] - was increased (Figs. 5h and S6a). Altogether, our data pointed to c-*Met* as a gene that could enhance lymphomagenesis in *MYC;Dnmt3b*$^{Cl/Cl}$ lymphomas.

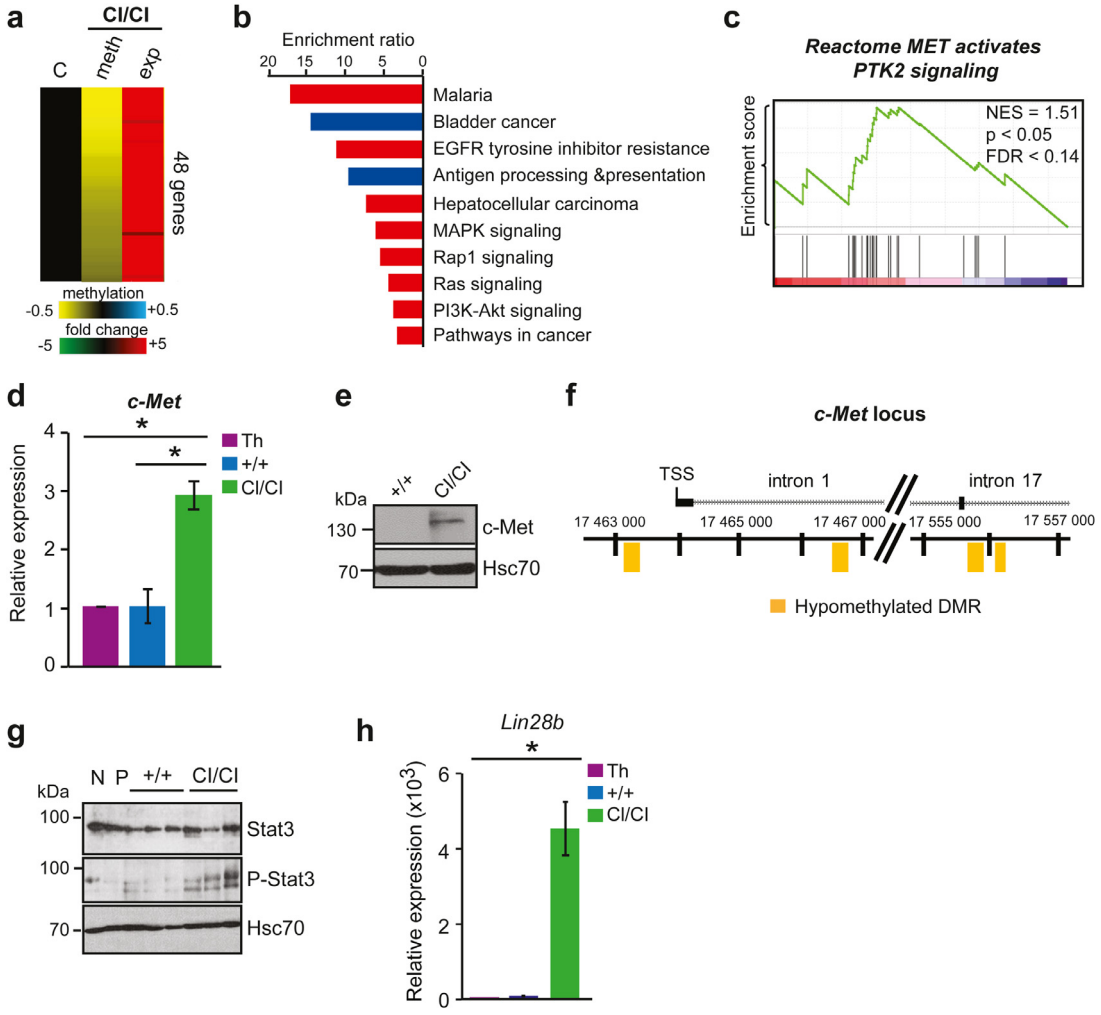

Fig. 5. Pathways associated with c-Met-oncogene are upregulated in *MYC;Dnmt3b*$^{Cl/Cl}$ lymphomas.

a. Heat map of genes with hypomethylated DMRs in promoters (meth. diff. ≥20%; p(MWU) <0.05) and overexpressed (FC≥2, $p<0.05$ by DESeq) specifically in *MYC;Dnmt3b*$^{Cl/Cl}$ but not in *MYC;Dnmt3b*$^{+/+}$ lymphomas when compared to control T-cells (C). b. KEGG pathway analysis of genes presented in (a). Red- pathways including c-Met, blue- without c-Met. c. GSEA shows positive enrichment in *MET activates PTK2 signalling* in *MYC;Dnmt3b*$^{Cl/Cl}$ lymphomas. Normalized enrichment scores (NES), false discovery rate (FDR) and p-values are shown. d. c-*Met* expression by real-time qRT-PCR in *MYC;Dnmt3b*$^{+/+}$ lymphoma ($n = 2$) and *MYC;Dnmt3b*$^{Cl/Cl}$ ($n = 3$) relative to normal thymus ($n = 2$). Data were normalized to *β-actin*. $^*p<0.05$. e. Immunoblot of c-Met and Hsc70 levels in *MYC;Dnmt3b*$^{+/+}$ and *MYC;Dnmt3b*$^{Cl/Cl}$ tumours. f. Schematic representation of hypomethylated DMRs in *c-Met* locus detected only in *MYC;Dnmt3b*$^{Cl/Cl}$ lymphomas as determined by WGBS. Numbers indicate chromosomal coordinates (mm10). TSS – transcription start site g. Immunoblot of Stat3, phospho-Stat3 and Hsc70 levels in *MYC;Dnmt3b*$^{+/+}$ and *MYC;Dnmt3b*$^{Cl/Cl}$ tumours. *MYC;Dnmt3b*$^{+/+}$ pre-tumour thymocytes isolated from 3-weeks old disease free mouse (P) and NIH 3T3 cell line (N) served as a control. h. *Lin28b* expression by real-time qRT-PCR in *MYC;Dnmt3b*$^{+/+}$ ($n = 2$) and *MYC;Dnmt3b*$^{Cl/Cl}$ ($n = 4$) lymphomas relative to control thymus ($n = 3$), Data are normalized to *β-actin*, $^*p = 0.007$.

All the data are presented as mean ±SEM, p-values were calculated by two-tailed Student's *t*-test.

3.6. *Activation of c-Met enhances lymphomagenesis in* Dnmt3b$^{Cl/Cl}$ *mice*

Because our molecular analysis suggested that *c-Met* oncogenic signalling is increased specifically in *MYC;Dnmt3b*$^{Cl/Cl}$ lymphomas, we next tested whether activation of this pathway in *MYC;Dnmt3b*$^{+/+}$ cell line will affect cellular growth *in vitro*. C-Met pathway activation can be achieved by the expression of c-Met cytoplasmic domain (cyto-Met) that has constitutive tyrosine kinase activity [43,44]. We first expressed either vector control expressing EGFP or cyto-Met tagged with EGFP in *MYC;Dnmt3b*$^{+/+}$ cell line and confirmed successful expression of cyto-Met in cells by immunoblot analysis (Fig. 6a). To assess effects of cyto-Met expression on growth, we monitored behaviour of EGFP+ cells by FACS over time. This analysis revealed that percentage of EGFP+ cells increased over time in cyto-Met expressing but not in control cells (Fig. 6b, c). These data suggest that cyto-Met expression enhances proliferation of *MYC;Dnmt3b*$^{+/+}$ cells.

Because c-Met activation can affect multiple downstream targets including PI3K pathway and STAT3 phosphorylation [38], we next analysed molecular changes present in cyto-Met expressing cells. This analysis revealed increased levels of Akt, phosphorylated Stat3 and decreased Stat5 (Fig. 6d). Downregulation of STAT5 oncogene in highly proliferative cells with Met activation was somewhat unexpected as this gene typically exerts oncogenic functions, but at least in some settings *e.g.* in a Myc-induced Acute B-Lymphoblastic Leukaemia/Lymphoma mouse model, it was also shown to have tumour suppressive functions [45]. In contrast, STAT3 phosphorylation is an oncogenic event that has been shown to be induced by c-MET through the direct binding followed by dimerization and STAT3 translocation to the nucleus supporting *e.g.* invasion of human squamous cell carcinoma line *in vitro* [38].

Exogenous expression of cyto-Met also increased Lin28b suggesting that this event may contribute to the enhanced cellular proliferation (Fig. 6e). Importantly, Lin28b overexpression in haematopoietic

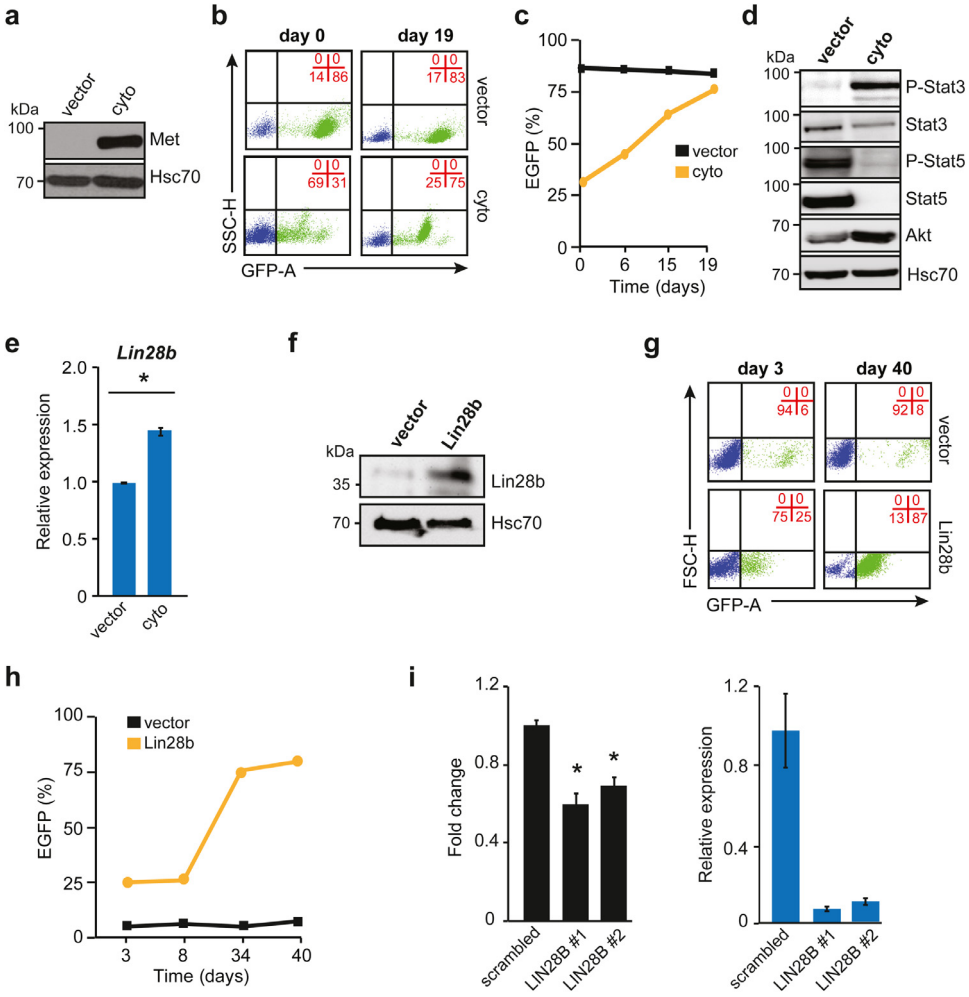

Fig. 6. c-Met signalling enhances proliferation and induces phospho-Stat and Lin28b.

a. Immunoblot of c-Met levels in mouse TCL line upon transduction with lentivirus encoding cyto-Met-EGFP (cyto) or vector-EGFP (vector). b. EGFP expression measured by FACS in mouse TCL line ectopically expressing cyto-Met-EGFP or vector-EGFP at 48 h after transduction (day 0) and 19 days later upon continuous culturing *in vitro*. The percentage of EGFP-positive and -negative cells is indicated. c. Percentage of EGFP-positive cells expressing cyto-Met-EGFP or vector-EGFP upon culturing *in vitro* at indicated times. d. Immunoblot of indicated proteins in mouse TCL line expressing cyto-Met-EGFP or vector-EGFP. e. *Lin28b* expression by real-time qRT-PCR in lymphoma cells expressing cyto-Met or vector-EGFP. Data are normalized to *β-actin* and presented as mean ±SEM from two independent experiments, $^*p = 0.002$. f. Immunoblot of Lin28b levels in mouse TCL line upon transduction with MSCV-Lin28b-EGFP or vector-EGFP. g. EGFP expression measured by FACS in mouse TCL ectopically expressing Lin28b-EGFP or vector-EGFP at indicated days after transduction. The percentage of EGFP-positive and -negative cells is indicated. h. Percentage of EGFP-positive cells expressing Lin28b-EGFP or vector-EGFP upon culturing *in vitro* at indicated times. i. *(left)* Cell proliferation of human TCL line HUT-78 transduced with lentivirus encoding two independent shRNA against LIN28B (LIN28B#1 and LIN28B#2) or *scrambled*, measured by MTT assay. Data are presented as mean ±SEM (from three independent experiments) relative to *scrambled*, $^*p = 0.047$. (*right*) *LIN28B* expression by real-time qRT-PCR in HUT-78 expressing shRNA targeting LIN28B or *scrambled* shRNA control. Data are normalized to *β-actin* presented as mean ± SEM (from three independent experiments).

All p-values were calculated by two-tailed Student's *t*-test.

cells results in development of peripheral T-cell lymphomas in transgenic mice [46], further supporting the idea that c-Met activation upregulating Lin28b may be relevant in accelerated lymphomagenesis observed in *MYC;Dnmt3b*$^{CI/CI}$ mice. To determine whether Lin28b expression affects mouse lymphoma growth, we next transduced *MYC;Dnmt3b*$^{+/+}$cells with control retroviruses expressing only EGFP or retroviruses expressing full-length Lin28b and EGFP (Fig. 6f). The percentage of EGFP+ cells increased over time in Lin28b overexpressing but not in control cells (Fig. 6g, h).

Pro-proliferative effect of LIN28b was further confirmed by shRNA-mediated knockdown in CTCL line HUT-78 that reduced cellular growth (Fig. 6i).

Taken together, our data suggest that activation of c-Met signalling *in vitro* promotes cell growth, upregulates phosphorylation of oncogenic Stat3 possibly promoting the cellular growth through upregulation of Lin28b. Thus, upregulation of c-Met transcription in the absence of Dnmt3b's CA may contribute to an accelerated lymphomagenesis observed in *MYC;Dnmt3b*$^{CI/CI}$ mice. However, only inactivation of the c-Met signalling pathway would determine the extent to which this pathway is involved in lymphomagenesis *in vivo*.

3.7. MET is upregulated in human T- and B-cell lymphomas

To determine whether MET signalling may contribute to disease in humans, we next analysed gene expression of 10 peripheral T-cell lymphomas (PTCLs) and controls by RNA-seq and combined results with publically available data on human lymphomas (Supplementary Data 3). This analysis identified 5275 upregulated and 717 downregulated genes (FC>3 fold, $p<0.05$ by DESeq) in hPTCL relative to normal T-cells (Figs. 7a and Supplementary Data 4). MET expression was elevated on average by ~58-fold in hPTCL (Fig. 7b) and a significant positive enrichment in *Seiden oncogenesis by MET* was detected by GSEA (Fig. 7c). Analysis of Hemap data set revealed that MET expression was not only elevated in T-cell Lymphoma (TCLs) but also BCLs, multiple myelomas (MM) and a subset of human cell lines, while its low expression was observed in AML, Chronic Myeloid Leukaemia (CML) and Chronic Lymphocytic Leukaemia (CLL) (Fig. 7d). To determine if MET downregulation affects cellular proliferation, we transduced human TCL line HH with constructs encoding shRNA against MET. Expression of two independent shRNA constructs resulted in significantly decreased proliferation of cells suggesting that MET expression is important for growth of these cells (Figs. 7e, f and data not shown).

To determine whether DNMT3B can function as a tumour suppressor in humans, we next analysed mutational spectrum in haematologic malignancies using Catalogue of Somatic Mutations in Cancer (COSMIC) [47]. This analysis revealed that genetic alterations such as deletions, substitutions, missense and nonsense mutations in coding region in *DNMT3B* locus were detected in variety of malignancies albeit at low frequencies. For example, DNMT3B is mutated in 12% of CTCL, 7% of therapeutic-related myelodysplastic syndrome (t-MDS), 1.3% of PTCL and 0.2% of AML (Fig. 7g, h). However, a close relative *DNMT3A* is mutated more frequently with especially in AML and PTCL (Fig. 7g, h). Given that DNMT3A has been shown to have shared functions with DNMT3B in several settings including haematopoietic organs and form complexes with DNMT3B [48-50], the alterations in either of the genes may affect DNMT3B activity.

Altogether our data suggest that DNMT3B's CA may be relevant in human haematologic malignancies by contributing to regulation of oncogenic signalling pathways including MET, in particular in PTCL and B-cell lymphomas.

4. Discussion

Hereby we provide direct genetic evidence that Dnmt3b's CA is critical for its tumour suppressor function in pathogenesis of mouse TCL and AML and it is also involved in suppression of MEFs transformation. A consequence of this finding is that through methylation, Dnmt3b's CA is associated with genomic elements causatively contributing to tumourigenesis at least in the tested biological settings. Our data further highlight the importance of aberrant hypomethylation in mouse haematologic malignancies.

Our results link Dnmt3b' CA to control of proto-oncogene c-Met [38]. This receptor tyrosine kinase is activated in epithelial and mesenchymal cells by binding HGF resulting in activation of RAS, PI3K/AKT, Wnt/β-catenin and STAT3 signalling pathways that are involved in embryonic development, organ morphogenesis and cell motility [51]. Aberrant activation of HGF/c−MET axis is seen in gastric, thyroid, pancreas and lung cancers [52,53]. Role of c-Met is not well understood in haematopoiesis but it is expressed primarily on CD34+ stem cells and may be involved in lineage commitment [54,55].

Several lines of evidence suggest that c-Met is a putative target of Dnmt3b's CA and its increase drives accelerated lymphomagenesis in mice. First, while *c-Met* is methylated and not expressed in normal T-cells, hypomethylation of its promoter, introns 1 and 17 is associated with ~25-fold increase in transcript levels in *MYC;Dnmt3b*$^{CI/CI}$ lymphomas suggesting de-repression upon methylation decrease. Consequently, activation of c-Met signalling was invariably identified by various bioinformatics tools including IPA, GSEA, KEGG in global gene expression profiles derived from *MYC;Dnmt3b*$^{CI/CI}$ lymphomas. Second, functional activation of c-Met signalling in lymphoma cells enhanced cellular proliferation, Stat3 phosphorylation and Lin28b expression. Stat3 regulates pro-proliferative genes, such as Cyclin D1 and c−Myc, and is involved in the progression of various cancers [56,57]. While the ability of STAT3 to directly activate LIN28B expression was observed during inflammation-stimulated epithelial-to-mesenchymal transition in prostate cancer [42], such link is not known to operate in lymphomas. Importantly, overexpression of Lin28b phenocopied c-Met activation in providing lymphoma cells proliferative advantage further supporting a relevance of this link. Our data suggest that c-Met activation results in Stat3 phosphorylation that, in turn, activates Lin28b. This concept is further supported by results showing that transgenic mice expressing oncogenic fusion protein Tpr-Met in thymocytes developed TCL with 100% penetrance [58], and also by findings that transgenic mice overexpressing Lin28b in haematopoietic cells develop PTCL [46]. Thus, c-Met-Stat3-Lin28b may work as a linear axis and functionally contribute to T-cell lymphomagenesis. Lastly, MET is upregulated in a subset of human PTCLs, BCLs and MMs, and its knockdown suppresses proliferation of TCL *in vitro*. Thus, Met pathway is likely relevant in human PTCL but further analysis is needed to elucidate whether MET activation predicts worse survival and whether MET inhibitors are useful in the treatment. While our data suggest that c-Met signalling may be involved in accelerated lymphomagenesis in *MYC;Dnmt3b*$^{CI/CI}$ mice, only future studies inactivating components of this pathway can provide an answer to its exact role in development of lymphomas.

Whether DNMT3B's CA plays a role in human TCL is unclear at the present time remains to be seen. Although infrequently, certain haematologic malignancies such as PTCL, CTCL, AML and t-MDS present with low frequency genetic alterations in *DNMT3B* locus. Mutations are more frequent in DNMT3A which is a binding partner of DNMT3B and therefore may affect its activity [59-62]. In addition, the inhibitor of DNMT3B - TCL1 protein [63] – is overexpressed in many haematologic malignancies, such as Follicular lymphoma, Burkitt lymphoma, DLBCL, CLL, T-cell prolymphocytic leukaemia [63,64] thus likely contributing to DNMT3B inhibition. It is therefore likely that DNMT3B is a tumour suppressor in human PTCL but further studies need to be performed to address this point.

In this study, we show that mice expressing Dnmt3b^{CI} survive postnatal development but suffer from ICF-like syndrome. Several features of *Dnmt3b*$^{CI/CI}$ mice are consistent with human ICF syndrome including facial anomaly, reduced body weight, reduction in total methylcytosine levels and haematopoietic defects, especially

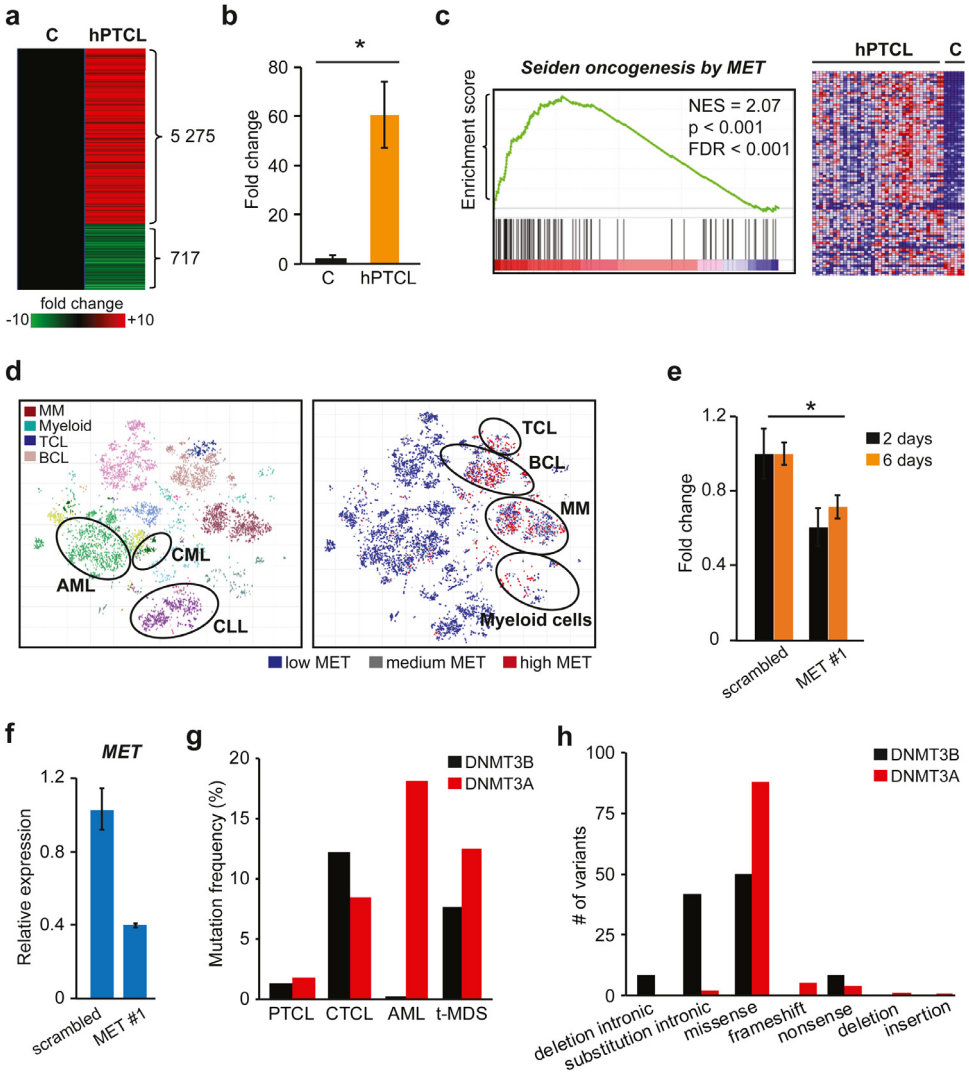

Fig. 7. *Dnmt3b's CA signature* is present in human haematologic malignancies.

a. Heatmap of differentially expressed genes (FC>3, $p<0.05$ by DESeq) derived from RNA-seq data of human PTCL tumours (hPTCL, $n = 38$) and compared to normal CD4+ and CD8+ *T*-cells (C, $n = 6$). **b.** Fold change *MET* expression by RNA-seq in human PTCL tumours ($n = 38$) compared to control CD4+ and CD8+ *T*-cells (C, $n = 6$); $^{*}p<0.05$ by DESeq. Data are presented as mean ±SEM. **c.** (*left*) GSEA using RNA-seq data shows positive enrichment in *Seiden oncogenesis by MET* in human PTCL tumours ($n = 38$) when compared to control CD4+ and CD8+ *T*-cells ($n = 6$). Normalized enrichment scores (NES), false discovery rate (FDR) and p-values are shown.

(*right*) Heatmap showing expression of 100 genes in hPTCLs ($n = 38$) and control CD4+ and CD8+ *T*-cells (C, $n = 6$) from *Seiden oncogenesis by MET* gene set. High expression is indicated by red while low expression is shown by blue. **d.** *(left)* The transcriptome data projected in 2D by t-SNE in the indicated cancer types, cell lines, and normal cell populations with each dot representing one sample (HEMAP). The separation between annotated disease types (indicated by colour) is shown for distinct clusters visible on the cancer map *(right)*. Visualization of MET on a t-SNE map, with red, blue and grey dots corresponding to high, low and medium scores of *MET* expression, respectively (right). **e.** Cell proliferation of TCL line HH transduced with lentivirus encoding either shRNA against MET or *scrambled* measured by MTT assay at indicated times. Data are presented as mean fold difference ±SEM (from three independent experiments), $^{*}p<0.05$ by two-tailed Student's *t*-test. **f.** *MET* expression by real-time qRT-PCR in HH cell line expressing shRNA targeting MET or *scrambled* shRNA control. Data are normalized to *β-actin* and presented as mean ±SEM (from three independent experiments). **g.** Percentage of samples with mutated DNMT3B or DNMT3A identified in Peripheral T-cell lymphoma (PTCL), Cutaneous T-cell lymphoma (CTCL), Acute myeloid leukaemia (AML) and therapeutic-related myelodysplastic syndrome (t-MDS) as obtained from COSMIC database. **h.** Total number of variants of indicated types in DNMT3B and DNMT3A identified in PTCL, CTCL, AML and t-MDS.

impaired lymphocyte development. Attempts to establish ICF model were previously done by generation of mice expressing single point mutations derived from ICF patients [65]. While mutant mice were born and had ICF like features, they were not viable with most mice dying within 24 h. In contrast, *Dnmt3b*$^{Cl/Cl}$ mice, like humans, survive postnatal development and therefore may serve as good models for understanding the aetiology of ICF syndrome and for the identification of target genes that are regulated by DNA methylation during development.

Contributors

K.L., P.N., J.O., and R.O. contributed to the data generation, editing and writing of the manuscript. A.A. contributed to the data generation and editing. A.R. contributed to the gene expression and DNA methylation processing. R.O. supervised the project. All authors read and approved the final manuscript.

Declaration of Competing Interests

The authors declare no competing interests.

Acknowledgments

The authors thank the Flow Cytometry and Bioinformatics core facilities of the Interdisciplinary centre for Biotechnology Research at the University of Florida. This study was supported by Department of

Anatomy and Cell Biology and Cancer centre at the University of Florida start-up funds, NIH/NCI Grant 1R01CA188561-01A1 (R.O.).

Data Sharing Statement

All relevant data are available from the corresponding author upon reasonable request. The WGBS and RNA-seq are deposited at the NCBI Gene Expression Omnibus database [GSE154451] [66].

Supplementary materials

Supplementary material associated with this article can be found, in the online version, at doi:10.1016/j.ebiom.2020.103191.

References

[1] Zhang T, Cooper S, Brockdorff N. The interplay of histone modifications - writers that read. EMBO Rep 2015;16(11):1467–81.
[2] Zhang Y, Charlton J, Karnik R, Beerman I, Smith ZD, Gu H, et al. Targets and genomic constraints of ectopic Dnmt3b expression. Elife 2018;7.
[3] McCabe MT, Brandes JC, Vertino PM. Cancer DNA methylation: molecular mechanisms and clinical implications. Clin Cancer Res 2009;15(12):3927–37.
[4] Celik H, Kramer A, Challen GA. DNA methylation in normal and malignant hematopoiesis. Int J Hematol 2016;103(6):617–26.
[5] Okano M, Bell DW, Haber DA, Li E. DNA methyltransferases Dnmt3a and Dnmt3b are essential for de novo methylation and mammalian development. Cell 1999;99(3):247–57.
[6] Robert MF, Morin S, Beaulieu N, Gauthier F, Chute IC, Barsalou A, et al. DNMT1 is required to maintain CpG methylation and aberrant gene silencing in human cancer cells. Nat Genet 2003;33(1):61–5.
[7] Pradhan S, Bacolla A, Wells RD, Roberts RJ. Recombinant human DNA (cytosine-5) methyltransferase. I. Expression, purification, and comparison of de novo and maintenance methylation. J Biol Chem 1999;274(46):33002–10.
[8] Ooi SK, Qiu C, Bernstein E, Li K, Jia D, Yang Z, et al. DNMT3L connects unmethylated lysine 4 of histone H3 to de novo methylation of DNA. Nature 2007;448(7154):714–7.
[9] Bachman KE, Rountree MR, Baylin SB. Dnmt3a and Dnmt3b are transcriptional repressors that exhibit unique localization properties to heterochromatin. J Biol Chem 2001;276(34):32282–7.
[10] Fuks F, Burgers WA, Godin N, Kasai M, Kouzarides T. Dnmt3a binds deacetylases and is recruited by a sequence-specific repressor to silence transcription. EMBO J 2001;20(10):2536–44.
[11] Haney SL, Hlady RA, Opavska J, Klinkebiel D, Pirruccello SJ, Dutta S, et al. Methylation-independent repression of Dnmt3b contributes to oncogenic activity of Dnmt3a in mouse MYC-induced T-cell lymphomagenesis. Oncogene 2015;34(43):5436–46.
[12] Duymich CE, Charlet J, Yang X, Jones PA, Liang G. DNMT3B isoforms without catalytic activity stimulate gene body methylation as accessory proteins in somatic cells. Nat Commun 2016;7:11453.
[13] Nowialis P, Lopusna K, Opavska J, Haney SL, Abraham A, Sheng P, et al. Catalytically inactive Dnmt3b rescues mouse embryonic development by accessory and repressive functions. Nat Commun 2019;10(1):4374.
[14] Li E, Bestor TH, Jaenisch R. Targeted mutation of the DNA methyltransferase gene results in embryonic lethality. Cell 1992;69(6):915–26.
[15] Blanco-Betancourt CE, Moncla A, Milili M, Jiang YL, Viegas-Péquignot EM, Roquelaure B, et al. Defective B-cell-negative selection and terminal differentiation in the ICF syndrome. Blood 2004;103(7):2683–90.
[16] Franceschini P, Martino S, Ciocchini M, Ciuti E, Vardeu MP, Guala A, et al. Variability of clinical and immunological phenotype in immunodeficiency-centromeric instability-facial anomalies syndrome. Report of two new patients and review of the literature. Eur J Pediatr 1995;154(10):840–6.
[17] Ehrlich M, Sanchez C, Shao C, Nishiyama R, Kehrl J, Kuick R, et al. ICF, an immunodeficiency syndrome: DNA methyltransferase 3B involvement, chromosome anomalies, and gene dysregulation. Autoimmunity 2008;41(4):253–71.
[18] Jin B, Tao Q, Peng J, Soo HM, Wu W, Ying J, et al. DNA methyltransferase 3B (DNMT3B) mutations in ICF syndrome lead to altered epigenetic modifications and aberrant expression of genes regulating development, neurogenesis and immune function. Hum Mol Genet 2008;17(5):690–709.
[19] Kiel MJ, Sahasrabuddhe AA, Rolland DCM, Velusamy T, Chung F, Schaller M, et al. Genomic analyses reveal recurrent mutations in epigenetic modifiers and the JAK-STAT pathway in Sézary syndrome. Nat Commun 2015;6:8470.
[20] Morin RD, Mendez-Lago M, Mungall AJ, Goya R, Mungall KL, Corbett RD, et al. Frequent mutation of histone-modifying genes in non-Hodgkin lymphoma. Nature 2011;476(7360):298–303.
[21] Hlady RA, Novakova S, Opavska J, Klinkebiel D, Peters SL, Bies J, et al. Loss of Dnmt3b function upregulates the tumour modifier Ment and accelerates mouse lymphomagenesis. J Clin Invest 2012;122(1):163–77.
[22] Peters SL, Hlady RA, Opavska J, Klinkebiel D, Pirruccello SJ, Talmon GA, et al. Tumour suppressor functions of Dnmt3a and Dnmt3b in the prevention of malignant mouse lymphopoiesis. Leukemia 2014;28(5):1138–42.
[23] Vasanthakumar A, Lepore JB, Zegarek MH, Kocherginsky M, Singh M, Davis EM, et al. Dnmt3b is a haploinsufficient tumour suppressor gene in Myc-induced lymphomagenesis. Blood 2013;121(11):2059–63.
[24] Shah MY, Vasanthakumar A, Barnes NY, Figueroa ME, Kamp A, Hendrick C, et al. DNMT3B7, a truncated DNMT3B isoform expressed in human tumours, disrupts embryonic development and accelerates lymphomagenesis. Cancer Res 2010;70(14):5840–50.
[25] Zheng Y, Zhang H, Wang Y, Li X, Lu P, Dong F, et al. Loss of Dnmt3b accelerates MLL-AF9 leukemia progression. Leukemia 2016;30(12):2373–84.
[26] Consortium EP. An integrated encyclopedia of DNA elements in the human genome. Nature 2012;489(7414):57–74.
[27] Afgan E, Baker D, Batut B, van den Beek M, Bouvier D, Cech M, et al. The Galaxy platform for accessible, reproducible and collaborative biomedical analyses: 2018 update. Nucleic Acids Res 2018;46(W1):W537–W44.
[28] Nicol JW, Helt GA, Blanchard SG, Raja A, Loraine AE. The Integrated Genome Browser: free software for distribution and exploration of genome-scale datasets. Bioinformatics 2009;25(20):2730–1.
[29] Jühling F, Kretzmer H, Bernhart SH, Otto C, Stadler PF, Hoffmann S. metilene: fast and sensitive calling of differentially methylated regions from bisulfite sequencing data. Genome Res 2016;26(2):256–62.
[30] Gao T, He B, Liu S, Zhu H, Tan K, Qian J. EnhancerAtlas: a resource for enhancer annotation and analysis in 105 human cell/tissue types. Bioinformatics 2016;32(23):3543–51.
[31] Krämer A, Green J, Pollard J, Tugendreich S. Causal analysis approaches in Ingenuity Pathway Analysis. Bioinformatics 2014;30(4):523–30.
[32] Pölönen P, Mehtonen J, Lin J, Liuksiala T, Häyrynen S, Teppo S, et al. Hemap: an Interactive Online Resource for Characterizing Molecular Phenotypes across Hematologic Malignancies. Cancer Res 2019;79(10):2466–79.
[33] Jiang YL, Rigolet M, Bourc'his D, Nigon F, Bokesoy I, Fryns JP, et al. DNMT3B mutations and DNA methylation defect define two types of ICF syndrome. Hum Mutat 2005;25(1):56–63.
[34] Gennery AR, Slatter MA, Bredius RG, Hagleitner MM, Weemaes C, Cant AJ, et al. Hematopoietic stem cell transplantation corrects the immunologic abnormalities associated with immunodeficiency-centromeric instability-facial dysmorphism syndrome. Pediatrics 2007;120(5):e1341–4.
[35] Dodge JE, Okano M, Dick F, Tsujimoto N, Chen T, Wang S, et al. Inactivation of Dnmt3b in mouse embryonic fibroblasts results in DNA hypomethylation, chromosomal instability, and spontaneous immortalization. J Biol Chem 2005;280(18):17986–91.
[36] Land H, Chen AC, Morgenstern JP, Parada LF, Weinberg RA. Behavior of myc and ras oncogenes in transformation of rat embryo fibroblasts. Mol Cell Biol 1986;6(6):1917–25.
[37] Peters SL, Hlady RA, Opavska J, Klinkebiel D, Novakova S, Smith LM, et al. Essential role for Dnmt1 in the prevention and maintenance of MYC-induced T-cell lymphomas. Mol Cell Biol 2013;33(21):4321–33.
[38] Organ SL, Tsao MS. An overview of the c-MET signaling pathway. Ther Adv Med Oncol 2011;3(1 Suppl):S7–S19.
[39] Knudsen BS, Vande Woude G. Showering c-MET-dependent cancers with drugs. Curr Opin Genet Dev 2008;18(1):87–96.
[40] Garcia-Guzman M, Dolfi F, Zeh K, Vuori K. Met-induced JNK activation is mediated by the adapter protein Crk and correlates with the Gab1 - Crk signaling complex formation. Oncogene 1999;18(54):7775–86.
[41] Rodrigues GA, Park M, Schlessinger J. Activation of the JNK pathway is essential for transformation by the Met oncogene. EMBO J 1997;16(10):2634–45.
[42] Guo L, Chen C, Shi M, Wang F, Chen X, Diao D, et al. Stat3-coordinated Lin-28-let-7-HMGA2 and miR-200-ZEB1 circuits initiate and maintain oncostatin M-driven epithelial-mesenchymal transition. Oncogene 2013;32(45):5272–82.
[43] Zhen Z, Giordano S, Longati P, Medico E, Campiglio M, Comoglio PM. Structural and functional domains critical for constitutive activation of the HGF-receptor (Met). Oncogene 1994;9(6):1691–7.
[44] Amicone L, Terradillos O, Calvo L, Costabile B, Cicchini C, Della Rocca C, et al. Synergy between truncated c-Met (cyto-Met) and c-Myc in liver oncogenesis: importance of TGF-beta signalling in the control of liver homeostasis and transformation. Oncogene 2002;21(9):1335–45.
[45] Wang Z, LG, Kang Z, Bunting S, Tse W, Bunting KD. STAT5 has tumour suppressor-like activity in a murine model of Myc-initiated acute b-lymphoblastic leukemia/lymphoma doi.org/10.1182/blood.V118.21.919.919 ed Blood 2011:919.
[46] Beachy SH, Onozawa M, Chung YJ, Slape C, Bilke S, Francis P, et al. Enforced expression of Lin28b leads to impaired T-cell development, release of inflammatory cytokines, and peripheral T-cell lymphoma. Blood 2012;120(5):1048–59.
[47] Tate JG, Bamford S, Jubb HC, Sondka Z, Beare DM, Bindal N, et al. COSMIC: the catalogue of somatic mutations in cancer. Nucleic Acids Res 2019;47(D1):D941–D7.
[48] Challen GA, Sun D, Mayle A, Jeong M, Luo M, Rodriguez B, et al. Dnmt3a and Dnmt3b have overlapping and distinct functions in hematopoietic stem cells. Cell Stem Cell 2014;15(3):350–64.
[49] Li JY, Pu MT, Hirasawa R, Li BZ, Huang YN, Zeng R, et al. Synergistic function of DNA methyltransferases Dnmt3a and Dnmt3b in the methylation of Oct4 and Nanog. Mol Cell Biol 2007;27(24):8748–59.
[50] Xu TH, Liu M, Zhou XE, Liang G, Zhao G, Xu HE, et al. Structure of nucleosome-bound DNA methyltransferases DNMT3A and DNMT3B. Nature 2020;586(7827):151–5.
[51] Demkova L, Kucerova L. Role of the HGF/c-MET tyrosine kinase inhibitors in metastasic melanoma. Mol Cancer 2018;17(1):26.
[52] Zhang Y, Xia M, Jin K, Wang S, Wei H, Fan C, et al. Function of the c-Met receptor tyrosine kinase in carcinogenesis and associated therapeutic opportunities. Mol Cancer 2018;17(1):45.

[53] Sierra JR, Tsao MS. c-MET as a potential therapeutic target and biomarker in cancer. Ther Adv Med Oncol 2011;3(1 Suppl):S21–35.
[54] Ratajczak MZ, Marlicz W, Ratajczak J, Wasik M, Machalinski B, Carter A, et al. Effect of hepatocyte growth factor on early human hemopoietic cell development. Br J Hematol 1997;99(1):228–36.
[55] Tesio M, Golan K, Corso S, Giordano S, Schajnovitz A, Vagima Y, et al. Enhanced c-Met activity promotes G-CSF-induced mobilization of hematopoietic progenitor cells via ROS signaling. Blood 2011;117(2):419–28.
[56] Mora LB, Buettner R, Seigne J, Diaz J, Ahmad N, Garcia R, et al. Constitutive activation of Stat3 in human prostate tumours and cell lines: direct inhibition of Stat3 signaling induces apoptosis of prostate cancer cells. Cancer Res 2002;62(22):6659–66.
[57] Abdulghani J, Gu L, Dagvadorj A, Lutz J, Leiby B, Bonuccelli G, et al. Stat3 promotes metastatic progression of prostate cancer. Am J Pathol 2008;172(6):1717–28.
[58] Accornero P, Lattanzio G, Mangano T, Chiarle R, Taulli R, Bersani F, et al. An *in vivo* model of Met-driven lymphoma as a tool to explore the therapeutic potential of Met inhibitors. Clin Cancer Res 2008;14(7):2220–6.
[59] Nguyen TB, Sakata-Yanagimoto M, Nakamoto-Matsubara R, Enami T, Ito Y, Kobayashi T, et al. Double somatic mosaic mutations in TET2 and DNMT3A-origin of peripheral T cell lymphoma in a case. Ann Hematol 2015;94(7):1221–3.
[60] Palomero T, Couronné L, Khiabanian H, Kim MY, Ambesi-Impiombato A, Perez-Garcia A, et al. Recurrent mutations in epigenetic regulators, RHOA and FYN kinase in peripheral T cell lymphomas. Nat Genet 2014;46(2):166–70.
[61] Abate F, da Silva-Almeida AC, Zairis S, Robles-Valero J, Couronne L, Khiabanian H, et al. Activating mutations and translocations in the guanine exchange factor VAV1 in peripheral T-cell lymphomas. Proc Natl Acad Sci U S A. 2017;114(4):764–9.
[62] Manso R, González-Rincón J, Rodríguez-Justo M, Roncador G, Gómez S, Sánchez-Beato M, et al. Overlap at the molecular and immunohistochemical levels between angioimmunoblastic T-cell lymphoma and a subgroup of peripheral T-cell lymphomas without specific morphological features. Oncotarget 2018;9(22):16124–33.
[63] Palamarchuk A, Yan PS, Zanesi N, Wang L, Rodrigues B, Murphy M, et al. Tcl1 protein functions as an inhibitor of de novo DNA methylation in B-cell chronic lymphocytic leukemia (CLL). Proc Natl Acad Sci U S A. 2012;109(7):2555–60.
[64] Paduano F, Gaudio E, Mensah AA, Pinton S, Bertoni F, Trapasso F. T-cell leukemia/lymphoma 1 (TCL1): an oncogene regulating multiple signaling pathways. Front Oncol 2018(8):317.
[65] Ueda Y, Okano M, Williams C, Chen T, Georgopoulos K, Li E. Roles for Dnmt3b in mammalian development: a mouse model for the ICF syndrome. Development 2006;133(6):1183–92.
[66] Edgar R, Domrachev M, Lash AE. Gene Expression Omnibus: NCBI gene expression and hybridization array data repository. Nucleic Acids Res 2002;30(1):207–10.